Measuring the TG-43 Parameters of Iridium-192 using Monte Carlo-based Dosimetry

A thesis submitted in partial
Fulfillment of the requirements for the degree of
Master of Science

By

Kenneth Fong

December 2019
Worcester Polytechnic Institute

This thesis is approved for recommendation to the Graduate committee.

Dr. David Medich
Thesis Director

Dr. Germano Iannacchione
Committee Member

Dr. Izabela Stroe
Committee Member

Measuring the TG-43 Parameters of Iridium-192 using Monte Carlo-based Dosimetry

A Thesis

Submitted to the Faculty

of the

WORCESTER POLYTECHNIC INSTITUTE

in partial fulfillment of the requirements for the

Degree of Master of Science

in

Physics

By

Kenneth Fong

Dr. David C. Medich, Advisor

Abstract

Radioactive sources used in brachytherapy must be dosimetrically characterized prior to clinical use as defined the TG-43 protocol. In our previous project, Gafchromic film dosimetry was used to experimentally obtain the anisotropy function for an M-19 iridium-192 brachytherapy seed being developed by Source Production Equipment Corp (St. Rose, LA). In this project, the Monte Carlo N-Particle Transport code (MCNP) was used to computationally obtain the full set of TG-43 parameters including the Dose Rate Constant, the Reference Dose Rate, the Radial Dose Function, and the Anisotropy Constant for the M-19 seed.

Acknowledgements

I would like to thank Dr. David Medich for advising this project and providing guidance and encouragement. I would also like to thank Justine Dupere and Shaun Marshall for setting up the computers used to run MCNP, guiding me in how to run it, and addressing any questions and concerns I had.

I would also like to thank Nicole Beinstein for her role in the project off of which this thesis is based. Furthermore, I must thank Germano Iannacchione and Izabela Stroe for taking the time to review and constructively critique my research as part of my thesis committee.

Contents

List of Figures

List of Tables

1 Introduction

Brachytherapy first came about in the early 1900s when various researchers discovered that tumors exposed to radiation would shrink. From then to the 1950s, brachytherapy was limited by factors such as the rarity of sufficiently radioactive materials and concerns over radiation exposure. Around the 1960s, the availability of the synthetic material iridium and remote afterloaders allowed brachytherapy to become a prominent cancer treatment that is safer and more effective for medical professionals to administer and patients to receive than surgical procedures (12).

Nonetheless, brachytherapy depends on radiation, which, in non-trivial doses, is inherently harmful to all tissues. Brachytherapy works by placing a radioactive source into a non-radioactive capsule to make a seed, and placing the seed such that more damage is dealt to cancerous tissues than to healthy tissues. To understand how a source and its emitted radiation used in brachytherapy will behave, they must be formally characterized.

1.A Goals

The goal of this thesis was to determine using the MCNP simulation code (17) the TG-43 dose rate parameters for the M-19 Ir-192 seed in an environment akin to the one used in our previous project. This will provide a basis of comparison between computational and experimental results, especially the anisotropy function calculated from our past experiment, and aid in the full characterization of this seed, which will make it eligible for FDA approval for clinical use.

1.B Background

1.B.1 Brachytherapy

Brachytherapy is a method of cancer treatment in which sealed radioactive sources are directly inserted near or into cancerous tissues. It proves most effective against tumorous cancers, especially prostate, breast, skin, and cervical cancers, since they have fixed, discernible locations in the body.

Three key factors considered when using brachytherapy are the placement of the source, the dose rate or intensity, and the dose duration. Ideally, the source will be placed such that its radiation will destroy the cancerous tissue while inflicting little harm on healthy tissues. The dose rate, measured in Grays per hour (Gy/h), can fall under four categories (19). Less than 2 Gy/h is considered low-dose rate (LDR). Between 2 and 12 Gy/h is considered medium-dose rate (MDR), commonly employed against tumors in the oral cavity and prostrate. Greater than 12 Gy/h is considered high-dose rate (HDR), commonly employed against tumors in the cervix, prostrate, breast, lung, and esophagus. Pulsed-dose rate (PDR) involves short, typically hourly pulses of radiation meant to produce the net effect of LDR, and it is commonly employed against tumors in the head and neck (10). The dose rate and duration are roughly inversely proportional, as LDR and PDR sources remain in the body for up to a day while HDR sources remain for only several minutes. (7)

1.B.2 Current Brachytherapy Practices

Modern brachytherapy relies heavily on remote afterloaders: machines that handle the transfer of sources into and out of the body, so as to minimize radiation exposure to medical personnel. More specifically, it is part of a whole apparatus: a lead pig holds the source, a catheter guides the source from the box to the target site in the body and back, and a programmable motor (the afterloader) pushes or pulls the source, attached to a wire, through the catheter. The desired placement of the source and dose duration are therefore controlled with the afterloader.

The source is always encased in a non-radioactive capsule, and the source and capsule combined are referred to as a brachytherapy seed. The desired dose rate is controlled by the type of seed or the number of seeds used. One variation of LDR treatment, called permanent brachytherapy, involves inserting small seeds (about a grain of rice in size) with a dose rate so low that the seeds need not be removed since the radioactivity of the source, over the course of weeks or months, decays to essentially zero (11).

Typically, the dosimetry of a source such as iridium-192 is done with thermoluminescent dosimeters, or TLDs. A TLD contains a thermoluminescent crystal, which, when exposed to heat from radiation, produces light, the intensity of which is used to measure radiation exposure (3). However, the lab used for this project generally works with ytterbium, which is relatively low in energy (average of 93 keV), and TLDs are not tissue equivalent at such low energies. This means that TLDs do not behave similarly to human tissues exposed to radiation when the energy from the source is too low.

1.B.3 Iridium-192 and the M-19 Seed

Iridium-192 has a half life of 73.83 days and an average energy of about 370 keV (14). It is a synthetic radioisotope, meaning it does not occur in nature. About 95% of iridium-192 goes through beta (β-) decay into platinum-192, and about 5% goes through electron capture into osmium-192 (4). Its decay scheme and Q value can be seen in Figure 1.2, and a selection of peak gamma energy values derived from the decay scheme is given in Table 1.1 (15). Iridium-192 is the standard source to use for brachytherapy. The experiment used the M-19 seed (see Figure 1.1), an HDR iridium-192 cylindrical source 0.350 cm in length and 0.065 cm in diameter encapsulated in a steel shell (5).

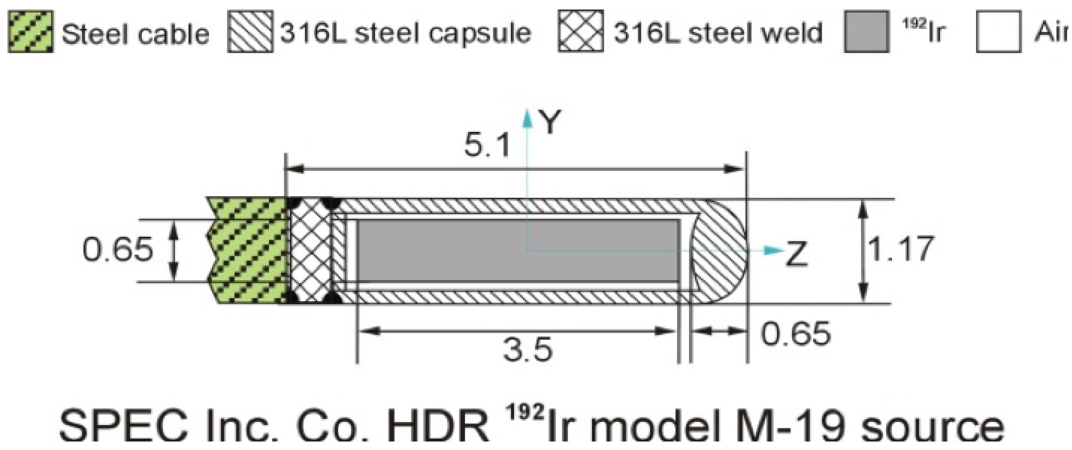

Figure 1.1: Diagram of the M-19 seed (5).

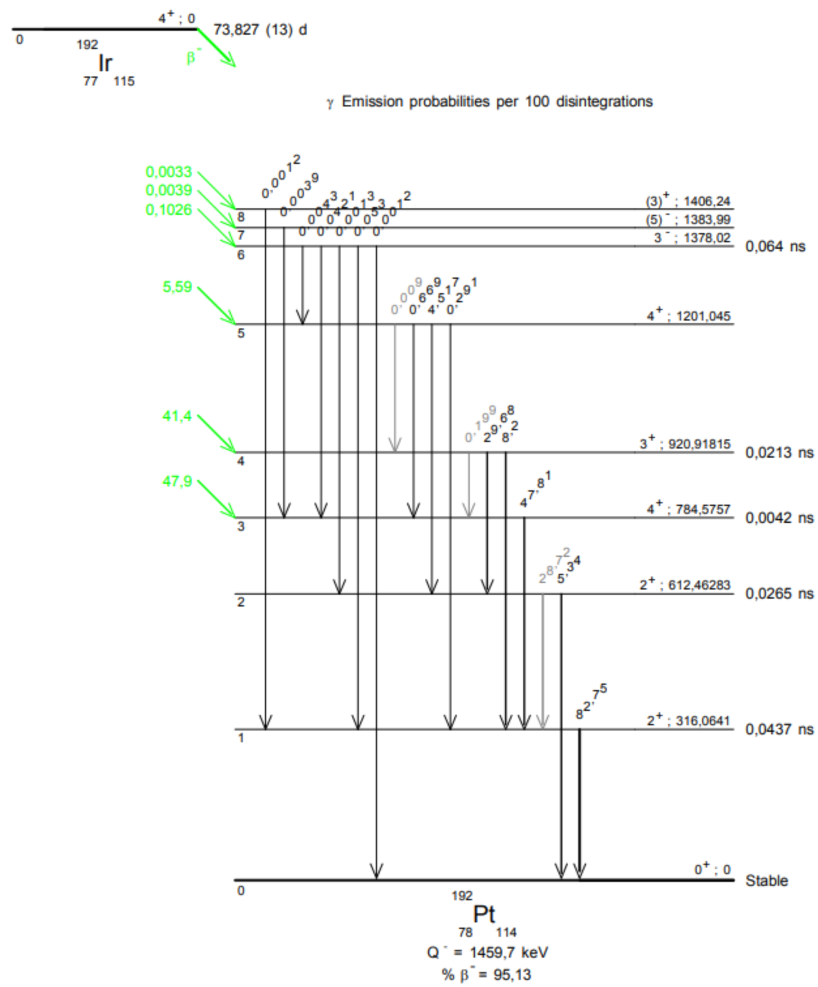

Figure 1.2: The decay scheme and Q value of iridium-192 (15).

Table 1.1: Peak gamma energy values for iridium-192 (15).

Energy (keV)	308	316	469	605	612
Intensity (%)	29.68	82.75	47.81	8.2	5.34

1.B.4 Gafchromic Film Dosimetry

In our past project, to ensure we could properly test and compare anisotropy (one of the TG-43 parameters) for both ytterbium and iridium, as well as any other sources of interest, we used EBT3 Gafchromic film, which is tissue equivalent, even at low energies, for experimental dosimetry (8). Gafchromic film dosimetry is done by irradiating the film, which darkens it, and using a computer and scanner to find the dark spots and their corresponding grayscale values. Additionally, Gafchromic film can be submerged in water to meet the TG-43 protocol (13), cut to size and shape as needed, easily calibrated, and analyzed with a 16-bit scanner and free image software.

Other completely separate MCNP results were compared to the results from Gafchromic film dosimetry, and aside from some measurements at low radii (especially $r = 1$ cm) or angles close to the edge of film, the results showed <10% difference between each other. Thus, for $r > 1$ cm and sufficiently large films, the feasibility of Gafchromic film dosimetry was demonstrated, and the anisotropy of the M-19 seed was characterized in the process.

1.C The TG-43 Parameters

Task-Group 43 (TG-43) of the American Association of Physicists in Medicine published and later updated a protocol to standardize brachytherapy dose calculations done both experimentally and computationally. Before a source can be used clinically, one must fully characterize it according to the TG-43 protocol, and to do so, five parameters, which taken together form a dose-rate equation, must be obtained: the geometry function, the radial dose function, the anisotropy function, the air-kerma strength, and the dose-rate constant (13).

1.C.1 The Geometry Function

Since the seed is roughly a minuscule right cylinder, it is best approximated as a line segment. The geometry function in a line-source approximation is given by:

$$G(r,\theta) = \begin{cases} \frac{\beta}{Lr\sin\theta} & \text{if} \quad \theta \neq 0^o \\ \frac{1}{r^2 - L^2/4} & \text{if} \quad \theta = 0^o \end{cases} \tag{1}$$

where L is the length of the seed, r is the distance between the center of seed and a point of measurement, and β is the subtended angle, as demonstrated in Figure 1.3 (16).

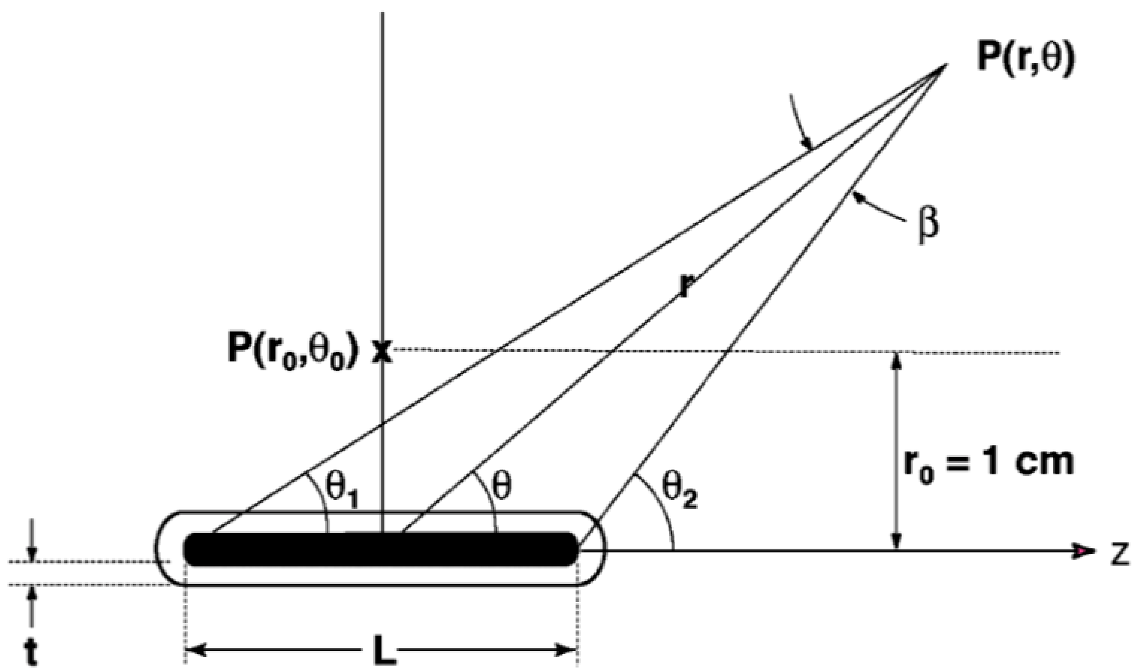

Figure 1.3: Subtended angle β used to calculate the geometry function of a seed (16).

So β can be formulated as:

$$\beta = \theta_1 - \theta_2 = \arctan\left[\frac{r\cos\theta + L/2}{r\sin\theta}\right] - \arctan\left[\frac{r\cos\theta - L/2}{r\sin\theta}\right] \tag{2}$$

1.C.2 The Radial Dose Function

The radial dose function according to the TG-43 protocol is given by:

$$g(r) = \frac{\dot{D}(r, \theta_0) \cdot G(r_0, \theta_0)}{\dot{D}(r_0, \theta_0) \cdot G(r, \theta_0)} \tag{3}$$

where $\dot{D}(r, \theta)$ is the dose rate and $G(r, \theta)$ is the geometry function. r_0 and θ_0, the reference distance and angle respectively, are defined by the protocol are 1 cm and $\pi/2$ radians respectively; the corresponding reference point $P(r_0, \theta_0)$ is also shown in Figure 1.3.

Physically, the radial dose function describes dose fall-off resulting from attenuation or scattering as a function of distance r from the source for points on its transverse plane, as defined by the protocol (16). This, however, excludes dose fall-off resulting from the spatial distribution of emitted radiation, which the geometry function alone accounts for.

1.C.3 The Anisotropy Function

The anisotropy function according to the TG-43 protocol is given by:

$$F(r, \theta) = \frac{\dot{D}(r, \theta) \cdot G(r, \theta_0)}{\dot{D}(r, \theta_0) \cdot G(r, \theta)} \tag{4}$$

where, likewise, $\dot{D}(r, \theta)$ is the dose rate and $G(r, \theta)$ is the geometry function.

Physically, the anisotropy of a brachytherapy source is a measurement of the deviation from the perfectly spherical spread of absorbed dose from a point source. The anisotropy function describes dose variation as a function of polar angle θ and distance r.

1.C.4 The Air-kerma Strength

The air-kerma strength, given in units of cGy·cm^2/h, is:

$$S_K = \dot{K}_\delta(d) d^2 \tag{5}$$

where d is the distance from the source center to a point of measurement on the transverse plane and $\dot{K}_\delta(d)$ is the air-kerma rate, i.e. the kerma-rate at a point in air, at d resulting from photons with energy greater than δ. The updated TG-43 protocol recommends excluding photons with energies less than this energy cutoff δ when calculating air-kerma strength because they do not meaningfully contribute to dose at distances larger than 0.1 cm (16). In the polar coordinate system used for the other parameters, $d = r$ provided that $\theta = \theta_0 = \pi/2$. d is generally chosen to be large enough relative to the dimensions of the source such that $\dot{K}_\delta(d)$ becomes roughly constant.

Physically, the air-kerma strength is simply the air-kerma rate without an implicit inverse square factor such that the relative magnitudes of air-kerma rates can be compared for different distances regardless of expected distance-based drop-off.

1.C.5 The Dose-rate Constant

The dose-rate constant, which simplifies to units of cm^{-2}, is:

$$\Lambda = \frac{\dot{D}(r_0, \theta_0)}{S_K} \tag{6}$$

where all arguments remain as defined earlier. Physically, the dose-rate constant represents the ratio between the dose rate at the reference point in water and the air-kerma strength.

1.C.6 The Dose-rate Equation

The five TG-43 parameters can be combined to construct the dose-rate equation (16):

$$\dot{D}(r, \theta) = S_K \cdot \Lambda \cdot \frac{G(r, \theta)}{G(r_0, \theta_0} \cdot g(r) \cdot F(r, \theta) \tag{7}$$

1.D Hypothesis

Our hypothesis is that Gafchromic film dosimetry can be used to measure the anisotropy function of a brachytherapy seed source, especially low energy sources, instead of thermoluminescent dosimeters. Based on our hypothesis, the specific aim of this thesis was to recreate the procedure used for Gafchromic film dosimetry in MCNP. The goal was to obtain through Monte Carlo simulations enough calculated dose values to obtain the TG-43 parameters as a basis of comparison for those same parameters experimentally obtained from future Gafchromic film dosimetry.

2 Methodology

2.A Summary of Experimental Design

The setup of this experiment was made up of a water tank, an afterloader, an iridium-192 brachytherapy seed attached to a wire and fed through a catheter, the films that were irradiated, and a holder for those films.

The design of the holder for Gafchromic film radiation dosimetry was done in a previous project. It was designed to hold the films between two half-cylindrical walls. The walls were inserted into half-circular notches in two base plates. The walls and corresponding notches were at incremental radii, from 1 cm to 10 cm. A rendering of the film holder can be seen in Figure 2.1.

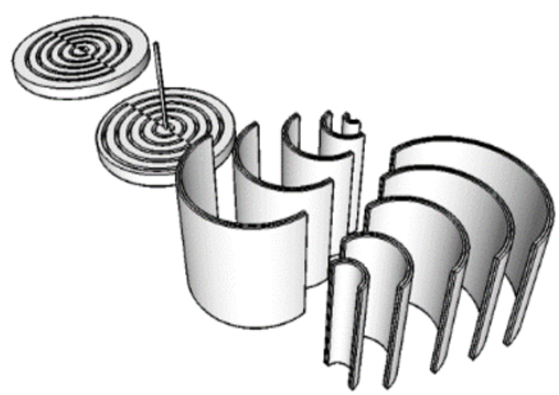

Figure 2.1: Rendering of the film holder design from SketchUp (6).

Once the holder was printed, holes were drilled on the edge of the base plates for cords to be fed through and attached to either end of the water tank. A weight was also attached to these wires to keep the holder submerged around the center of the tank for the entire experiment, such that the films and source could be surrounded by at least 30 cm of water on all sides, as dictated by the TG-43 protocol (13). Since human tissue is mostly comprised of water, the attenuation due to the water is similar to the attenuation due to tissue (20). Surrounding the source and the film in water also helps to account for scatter.

The source needed to be fed through the side of the cylinder created by the walls and base plate of the film holder. To accomplish this, a catheter was fed from the afterloader through the lead pig holding the source, across the tank, and attached to a fixed point on the other end of the tank. A semi-circular piece of sturdy plastic was placed in the holes at the center of the base plates, and the catheter was taped to the center point. The source tail was fed through the catheter, and the other end of the wire was fed into the afterloader.

The afterloader was a computer-controlled motorized crank. It was programmed to push the wire source tail a specific distance, which moved the source from the lead pig to the center of the tank. The computer then waited a specific amount of time, before pulling the source back into the lead pig. This process was used to limit the amount of exposure to the users. The original paper more thoroughly discusses the procedure and results of this experiment, such as calibration of the Gafchromic film and the formalism for obtaining dose values (6).

The entire setup can be seen in Figure 2.2, and example scans of the Gafchromic film can be seen in Figure 2.3.

Figure 2.2: An image of the water tank, lead pig, afterloader, and catheter and wire running through it all (left). A top view of the tank, showing the film holder submerged in the water (right) (6).

Figure 2.3: Scans of the Gafchromic film placed 3 cm from the seed before exposure (top) and after exposure (bottom) (6).

2.B MCNP Simulation

Simulation runs of input code were completed using MCNP6, 1.0 (17) on a two-computer cluster. The objective was to write up an input code that would roughly replicate the experimental design in an MCNP simulation. The code went through several iterations before a final version was decided upon. With each iteration I sought to add extra layers of reasonable complexity to the problem to better simulate the original experiment.

2.B.1 First Iteration

The initial priority was replicating the geometry of the experimental procedure by defining a basic geometric model in MCNP. As such, very many liberties were taken in designing the model. This model only accounts for measurements at $r = 1$ cm and assumes the following:

- The source and all cells (user-defined regions) are centered at the origin
- The water tank is a water-filled cube with a 100 cm side length; everything outside this cube is a particle graveyard
- The film is a water-filled cylindrical shell parallel to the x-axis with a 0.95 cm inner radius, 1.05 cm outer radius, and 20 cm height
- The source is a 0.35 cm long line segment parallel to the x-axis emitting photons of energy 0.38 MeV

A basic F6-type tally, which measures absorbed dose in MeV/g, was done on the whole film, partly as a code placeholder to minimize warnings in the run and partly for potential future reference. Likewise, the source was set to have a placeholder energy of 0.38 MeV (roughly the average energy of Ir-192) and a placeholder shape of a 1-D line segment (rather than the more accurate cylinder). This model suggests that the film has a uniform thickness of 1 mm, despite the likelihood of the physical deformation of bent film in a real-world application. Also, the film is taken to be a whole cylindrical shell in MCNP, whereas the actual films used in the experiment were less than half-cylindrical shells. Furthermore, with the film being tissue equivalent and tissue being sufficiently similar to water for attenuation purposes, the film in MCNP is made of water.

Aside from the incorrect orientation of the film, which should have been parallel to the z-axis, this iteration accurately captured the basic idealized geometric model without any computer errors. This iteration, complete with comments, is given in Appendix A.A.

2.B.2 Subsequent Iterations

Following the first iteration were a plethora of changes done to refine the geometric model and ensure fairly accurate and representative dose measurements. One attempted change was to include a plane normal to the y-axis to bisect the films and more closely approximate the actual films. This attempt failed as an error would occur when including this plane in the cell definition of a film. One successful change was to convert the line-source seed into a full-fledged cylinder encompassing three distinctly defined layers.

After finalizing the problem geometry, the focus of later iterations shifted to dictating where and how MCNP should extract dose absorption data from the final model. I decided to use a TMESH type 3 function that outputs the dose as MeV/cm^3/source particle in mesh cells defined by cylindrical surfaces; a simple conversion of these values with the density of water would yield true dose in MeV/g/source particle. A couple of unsuccessful attempted methods to use TMESH included:

- Defining the boundaries of the mesh cells at the points of measurements, e.g. placing a cell boundary at $r = 1$ cm, instead of defining boundaries to create small volumes around points where $r = 1$ cm
- Constructing a mesh where mesh cells were defined to be completely coincident with the cylindrical shells
  - This definition would have only output the absorbed dose over the whole film again, contrary to the objective of obtaining dose at different angles
  - Also a line overflow error occurred since each line in MCNP only supports 80 characters, a limit exceeded by this definition; attempts to make a multi-line TMESH card also failed

A major concern which arose with use of TMESH was the relative disorganization of values in the mctal output file, especially without access to the entire MCNP6 software suite to easily process the mctal file. Data appeared in the mctal file as an unlabeled, many-lined list of dose and error pairs of values, with 4 pairs per line. An early attempt to address this issue involved switching to a different tally altogether, the FMESH type 4 tally, which measures energy flux through surfaces; though this tally exists in the final iteration of the code, its output data was ultimately not used for analysis. The workaround I decided upon utilized multiple TMESH functions defined to produce multiple psuedo-tables of output data (explained in next section).

2.B.3 Final Iteration

The following is the totality of adjustments to the first geometric model which ultimately yielded the final model:

- The first film ($r = 1$ cm) is now parallel to the z-axis
- There exist films at other radii ($r = 2, 3, ...10$ cm) that are also water-filled cylindrical shells sharing the central axis and 20 cm height of the first
- All films have inner and outer radii given by $r - 0.05$ cm and $r + 0.05$ cm respectively
- The source (still parallel to x-axis) now consists of three distinct volumes:
  - An Ir-192-filled cylinder of 0.0325 cm radius and 0.35 cm height
  - A steel-filled and capped cylindrical shell of 0.0355 cm inner radius, 0.352 cm inner base, 0.0585 cm outer radius, and 0.510 cm outer base
  - A vacuum-filled space between the two aforementioned volumes
- The energy spectrum of Ir-192 has been defined

I selected the region of measurement in the TMESH to be the "central slice" of the films defined above, i.e. the 0.1 cm tall region within the films between the planes $z = -0.05$ cm and $z = 0.05$ cm. So final the TMESH model was defined as follows:

- Five TMESH functions were used, each measuring the central slice of two consecutive films; the workaround mentioned in the last section forces the dose and error values in the inner and outer films to always be the second and fourth data pairs of each line
- Each central slice was subdivided into 180 equally sized arc-like mesh cells of interest

- Mesh cells of interest exist at $\theta = t^\circ$, where t is an integer and $1 \leq t \leq 180$; their angular boundaries exist at $\theta = (t - 0.5)^\circ$ and $\theta = (t + 0.5)^\circ$

The final iteration of the code is given in Appendix A.B, and reference visuals created by plainly opening this code in the Visual Editor for MCNP (Visplot61_25) are given in Appendix E (18).

2.B.4 Supplementary Codes: Air-kerma strength and Dose-rate constant

For simplicity, kerma was assumed to be the same as absorbed dose because the two values generally have a $< 2\%$ difference between each other, and this difference is even smaller at distances greater than 0.1 cm. To run a simulation of an air-kerma measurement, the source (in its final iteration and position) was placed in a spherical vacuum 100 cm in radius. A small sphere of air 0.05 cm in radius was centered on the y-axis 10 cm away from the source; a similar air sphere was centered at $y = -1$ cm for reference, and an F6-type tally, which outputs dose in a a defined region in MeV/g, was done on both cells. Furthermore, the tally was set to run for 100 minutes of computer time to obtain with absolute certainty the irradiation time and by extension the air-kerma rate. Using Equation 5, the S_K values for both air spheres were found to have a 1.25% difference between each other, so the value at $y = 10$ cm was chosen as the roughly distance-independent value of S_K. Thus distance d was chosen to be 10 cm.

The code to obtain a dose-rate constant only required that absorbed dose at the reference point $P(r_0, \theta_0)$ be measured. In this code, the same source was placed in a sphere of water 100 cm in radius, and an F6-type tally was done for 100 minutes of computer time on a much smaller water sphere 0.05 cm in radius and centered at $y = 1$ cm (i.e. reference point P).

The codes to output the values used to calculate the air-kerma strength and dose-rate constant can be found in Appendices A.C and A.D respectively.

2.C Calculation Process

The default energy cutoffs of MCNP were used in the main TMESH code; I used the output dose values of the main code (Appendix A.B) to calculate the radial dose function and anisotropy function. Small energies (<1 keV for photons; <20 keV for electrons) were excluded in the supplementary codes; I used the output dose values of the supplementary codes (Appendices A.C and A.D) to calculate the air-kerma strength and dose-rate constant. Using the density of water at 25 °C (0.997 g/cm^3), dose in MeV/g/source particle was obtained from the TMESH. Raw output data from the TMESH is given in Appendix D.

2.C.1 Geometry Function

The geometry function $G(r, \theta)$ was calculated using Equation 1:

$$G(r,\theta) = \begin{cases} \frac{\beta}{Lr\sin\theta} & \text{if} \quad \theta \neq 0^o \\ \frac{1}{r^2 - L^2/4} & \text{if} \quad \theta = 0^o \end{cases}$$

where $L = 0.35$ cm and β is explained in Section 1.C.1.The geometry function used for MCNP calculations remained unchanged from that used for the original experiment since the same M-19 seed was used.

2.C.2 Radial Dose Function

The radial dose function $g(r)$, which involves $G(r, \theta)$, the dose rate $\dot{D}(r, \theta)$, the reference distance $r = 1$ cm, and the reference angle $\theta = 90°$, was calculated using Equation 3:

$$g(r) = \frac{\dot{D}(r, \theta_0) \cdot G(r_0, \theta_0)}{\dot{D}(r_0, \theta_0) \cdot G(r, \theta_0)}.$$

The dose rate $\dot{D}(r, \theta)$ is normally calculated by dividing the dose by the irradiation time. However, for dose values obtained from the TMESH tally, this is redundant since every point

$P(r,\theta)$ of measurement (or mesh cell of interest) is irradiated by the source for the same duration simultaneously. The irradiation times that go into the numerator and denominator of $g(r)$, being equal, cancel each other out, and the dose rate can thus be directly substituted with the dose values from TMESH for radial dose calculations.

2.C.3 Anisotropy Function

The anisotropy function $F(r,\theta)$ was calculated using Equation 4:

$$F(r,\theta) = \frac{\dot{D}(r,\theta)\cdot G(r,\theta_0)}{\dot{D}(r,\theta_0)\cdot G(r,\theta)}.$$

As with the radial dose calculations, the dose rate can be substituted with the dose values from TMESH for anisotropy calculations. Comparison of the MCNP anisotropy results to those from Gafchromic film dosimetry was done with a simple percent difference calculation, using the latter results as the reference. Note that two different scanners were used in the original experiment, so two sets of Gafchromic film dosimetry results are referenced.

2.C.4 Air-kerma Strength and Dose-rate Constant

The air-kerma strength S_K and the dose-rate constant Λ, both constants, were calculated using Equations 5 and 6 respectively.

$$S_K = \dot{K}_\delta(d)d^2 \qquad \Lambda = \frac{\dot{D}(r_0,\theta_0)}{S_K}$$

where, based on my assumption that kerma and dose are equal for S_K, I set $\dot{K}_\delta(d) = \dot{D}(r,\theta_0)$. I obtained $\dot{D}(r,\theta_0)$ by dividing the measured dose in a cell 10 cm from the source by the irradiation time explicitly defined in the code to be 100 minutes.

In calculating the dose-rate constant, two dose rate values are required, but as with the radial dose and anisotropy calculations, the irradiation times used in the numerator and denominator of Λ are equal are therefore irrelevant.

3 Results

3.A Geometry Function

For ease of comparing the geometry function at different r values, the values of the function itself were scaled up by r^2 to yield values equal to $G(r,\theta) * r^2$. Thus, the values of the geometry function times distance squared at all measured regions is given in Appendix B.

3.B Radial Dose Function

The radial dose values are also scaled up by r^2 for ease of comparison. The maximum percent error for the measured dose values and by extension the derived radial dose values was less than 3%. Since the general percent error for all data in MCNP is about 2%, the overall percent error was estimated to be $(\sqrt{3^2+2^2})\% \approx 3.61\%$. To err on the side of caution, I chose to round it up to 4%, and the error bars given in the graph in Figure 3.1 reflect this.

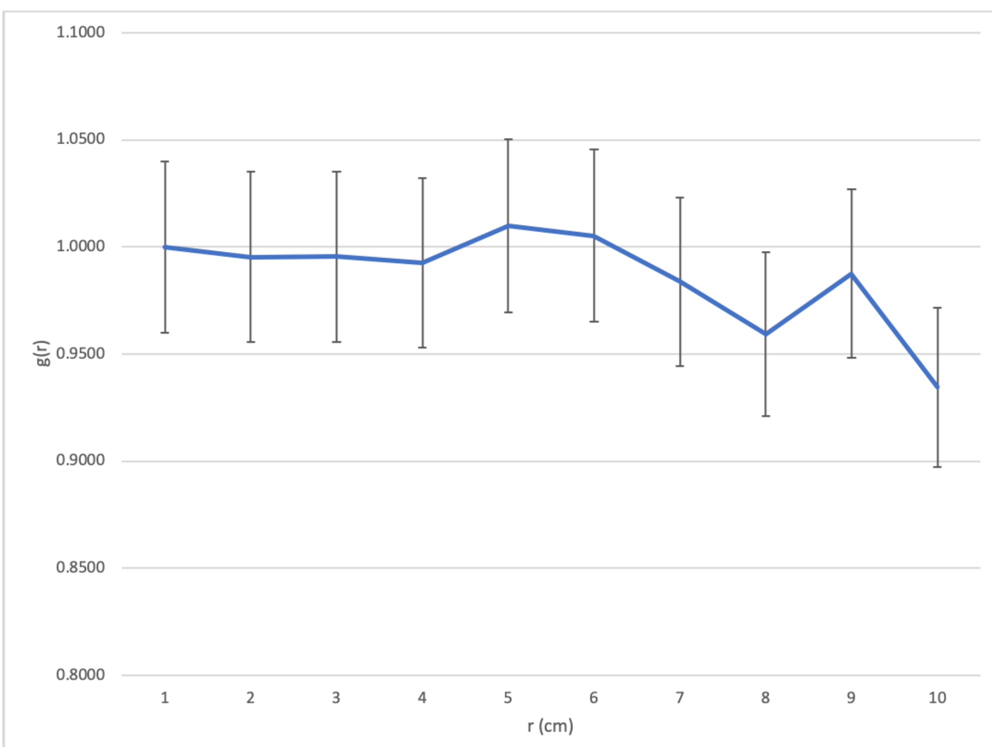

Figure 3.1: Graph of radial dose times distance squared. The error bars are all ± 4%.

Table 3.1: Radial dose function times distance squared for the M-19 seed in MCNP.

r	1	2	3	4	5	6	7	8	9	10
$g(r)$	1.0000	0.9952	0.9954	0.9926	1.0097	1.0052	0.9838	0.9593	0.9875	0.9344

3.C Anisotropy Function

Tabulated MCNP anisotropy values are given in Table C.1 of Appendix C. The MCNP anisotropy results were compared to the results, or rather, the two sets of results derived from the two different scanners used in our previous experiment (6). The percent difference of the MCNP values from each set of experimental values is tabulated in Tables C.2 and C.3 of Appendix C, and the two sets of anisotropy plots from the experiment overlaid with corresponding MCNP anisotropy plots are shown in Figures 3.2-3.11. Note that the plots from the experiment only cover angles from 40° to 140° because of the limitations of the films, the setup, the scanners, and the analysis software.

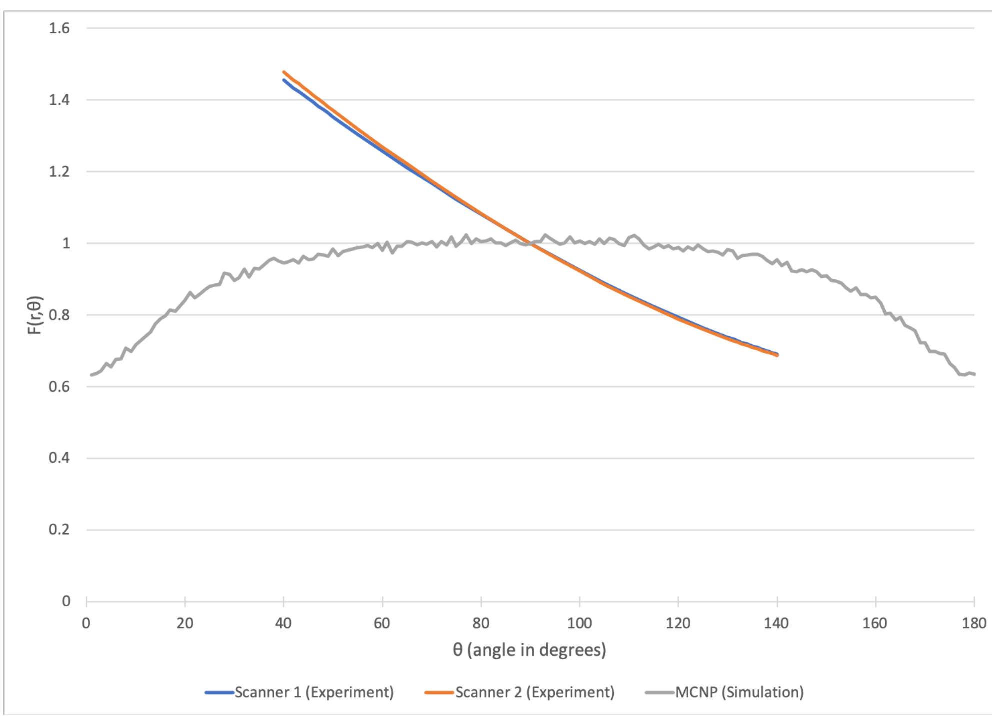

Figure 3.2: Anisotropy function at r=1 cm obtained from experiment and from simulation. The MCNP values are plotted against the values from Scanner 1 and Scanner 2.

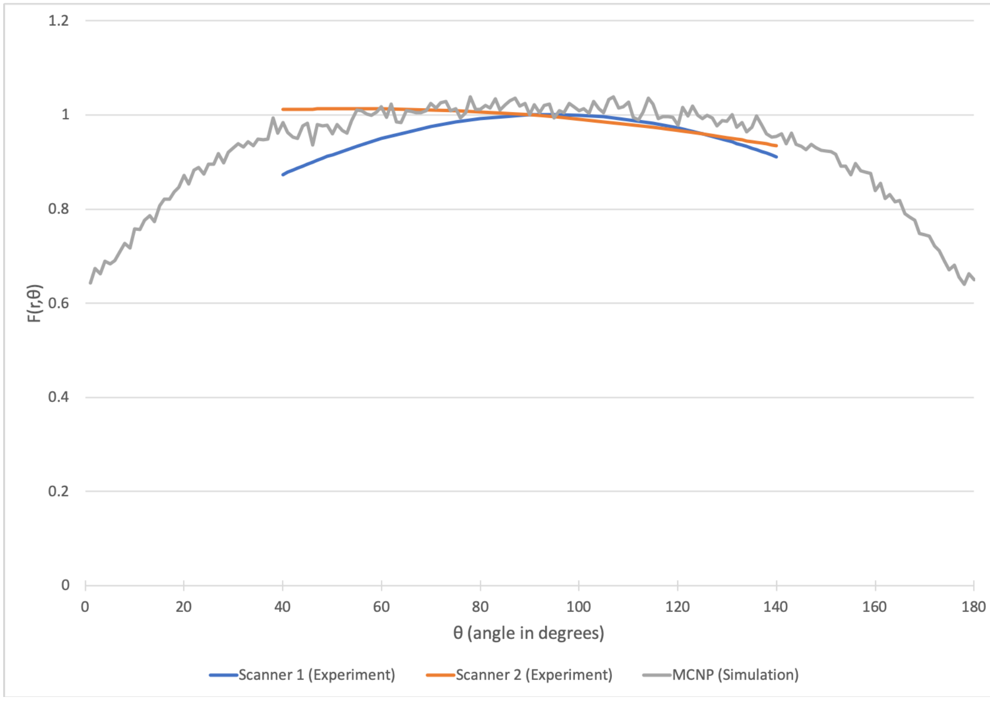

Figure 3.3: Anisotropy function at r=2 cm obtained from experiment and from simulation. The MCNP values are plotted against the values from Scanner 1 and Scanner 2.

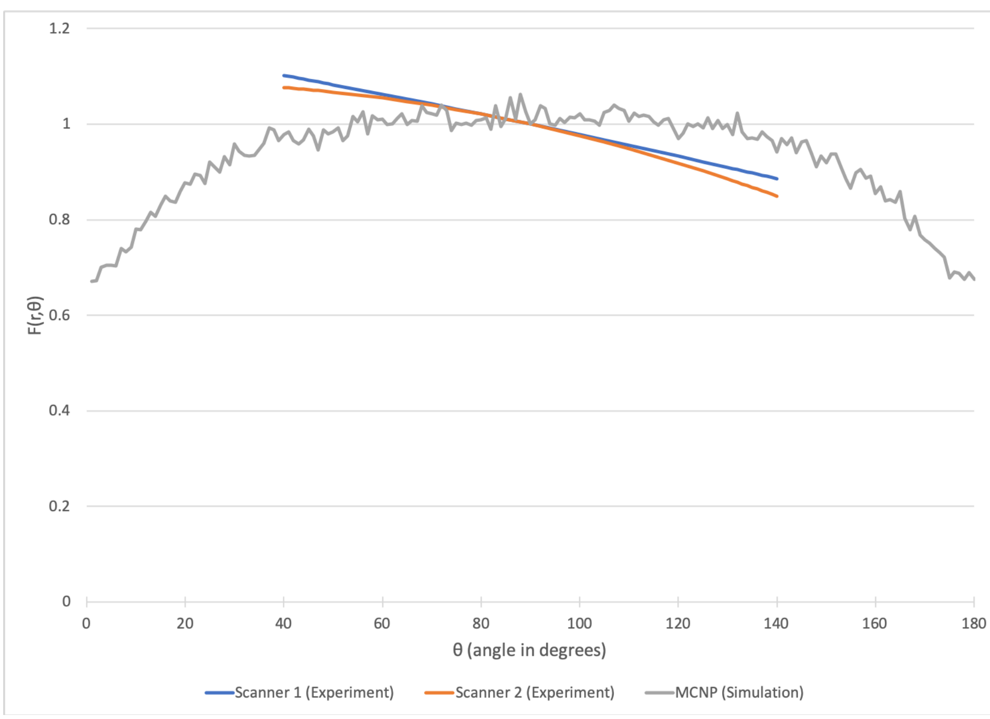

Figure 3.4: Anisotropy function at r=3 cm obtained from experiment and from simulation. The MCNP values are plotted against the values from Scanner 1 and Scanner 2.

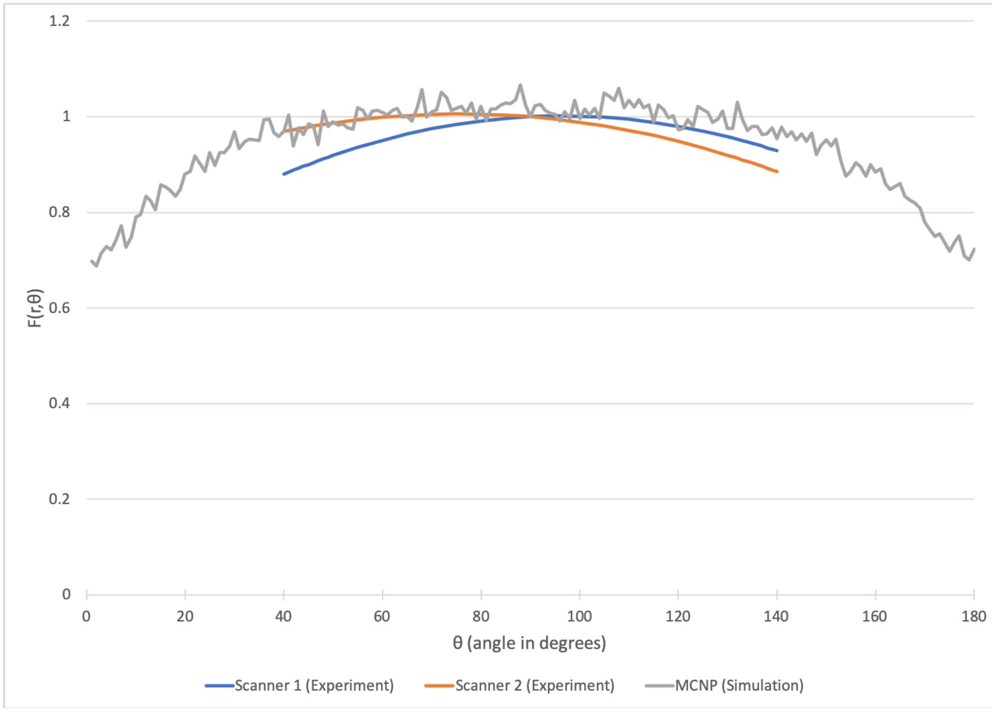

Figure 3.5: Anisotropy function at r=4 cm obtained from experiment and from simulation. The MCNP values are plotted against the values from Scanner 1 and Scanner 2.

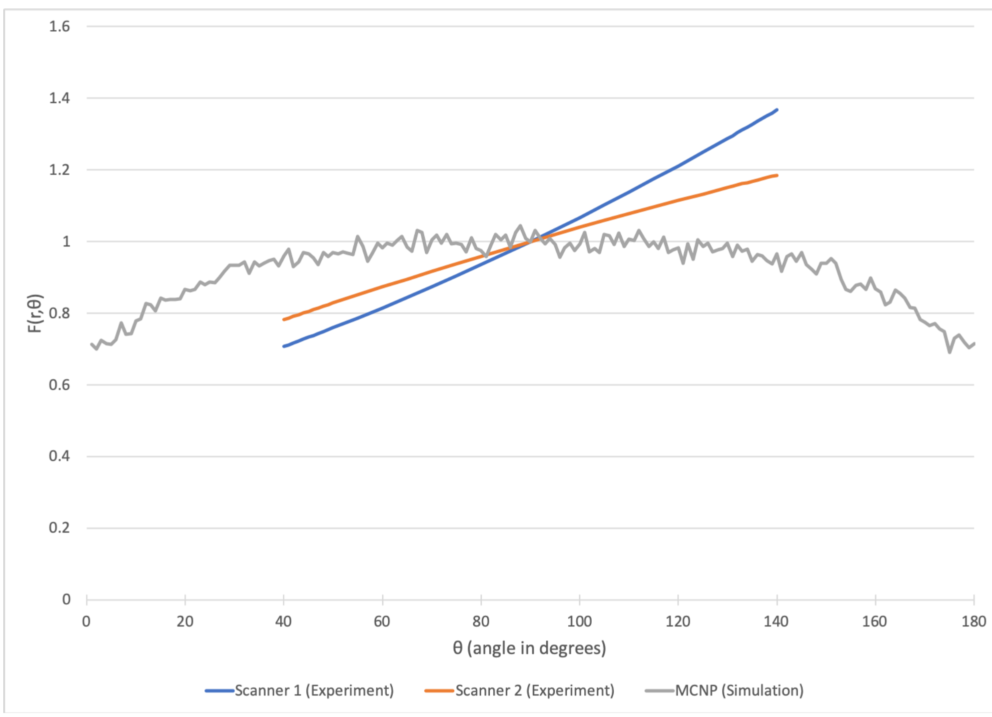

Figure 3.6: Anisotropy function at r=5 cm obtained from experiment and from simulation. The MCNP values are plotted against the values from Scanner 1 and Scanner 2.

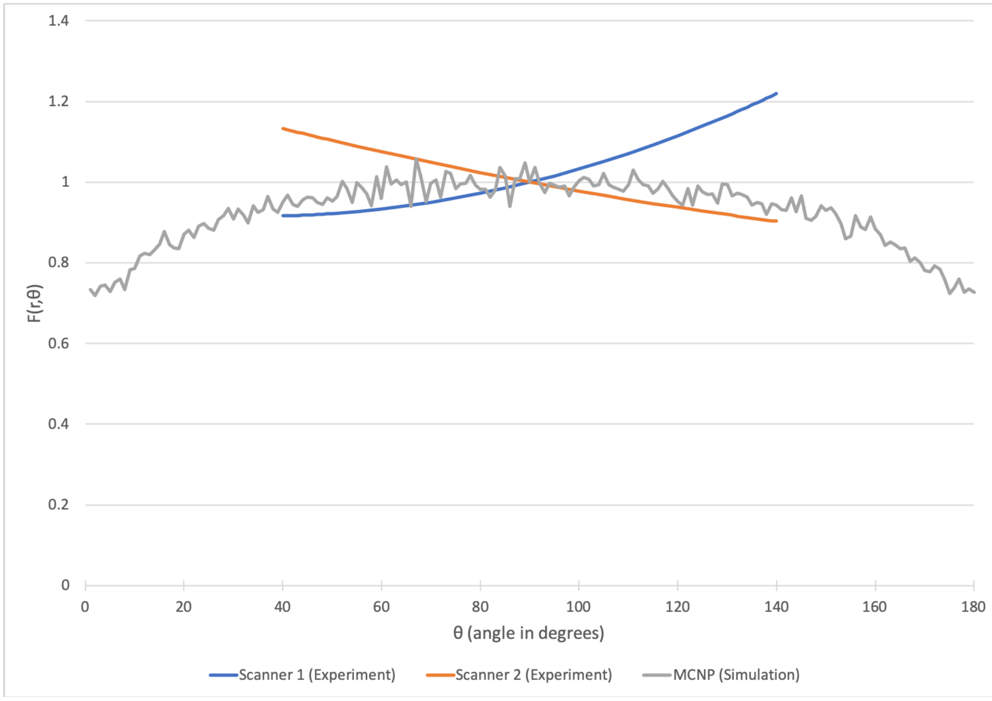

Figure 3.7: Anisotropy function at r=6 cm obtained from experiment and from simulation. The MCNP values are plotted against the values from Scanner 1 and Scanner 2.

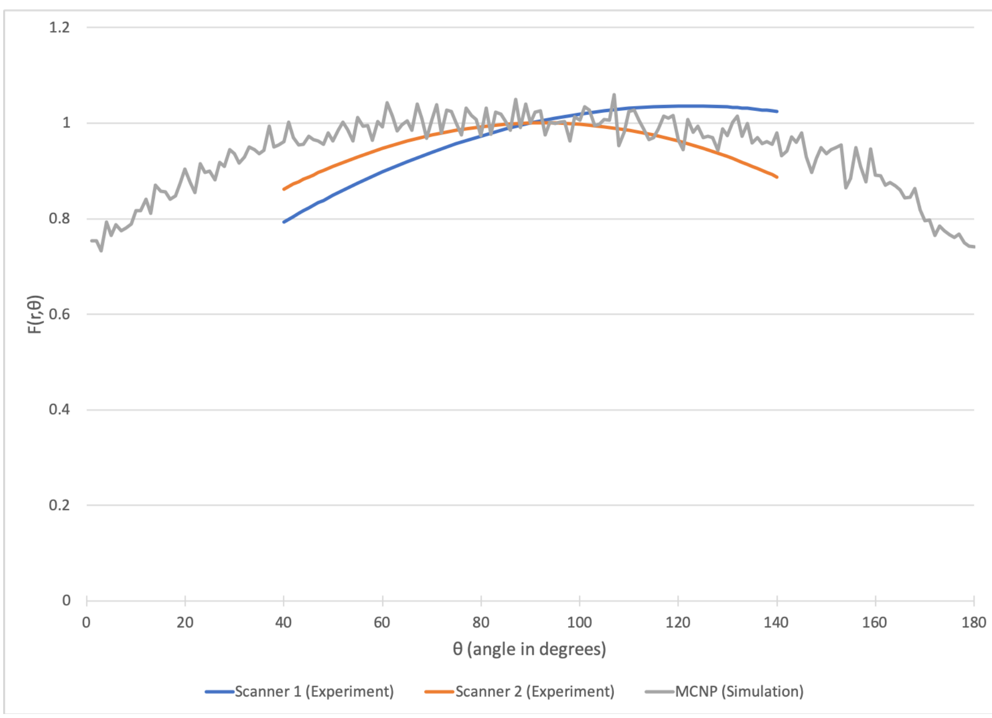

Figure 3.8: Anisotropy function at r=7 cm obtained from experiment and from simulation. The MCNP values are plotted against the values from Scanner 1 and Scanner 2.

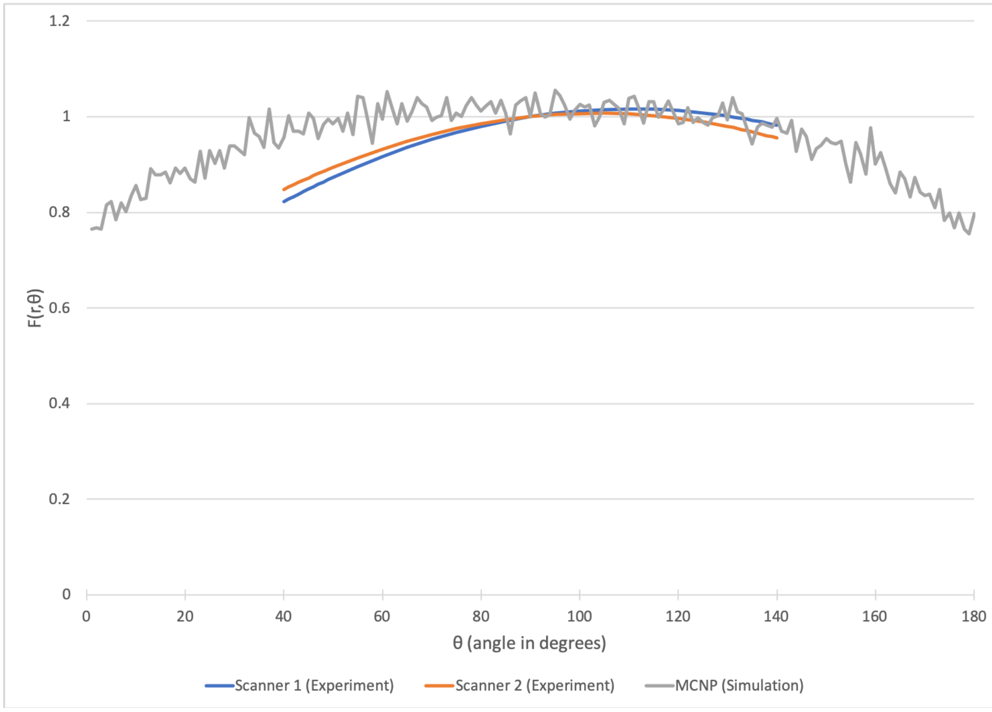

Figure 3.9: Anisotropy function at r=8 cm obtained from experiment and from simulation. The MCNP values are plotted against the values from Scanner 1 and Scanner 2.

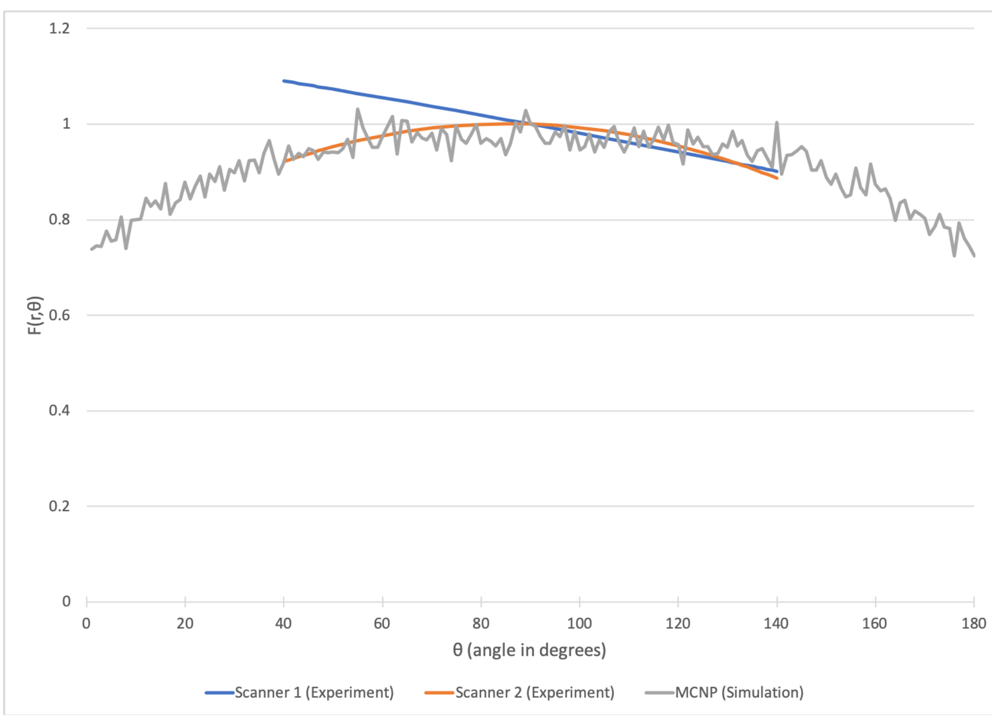

Figure 3.10: Anisotropy function at r=9 cm obtained from experiment and from simulation. The MCNP values are plotted against the values from Scanner 1 and Scanner 2.

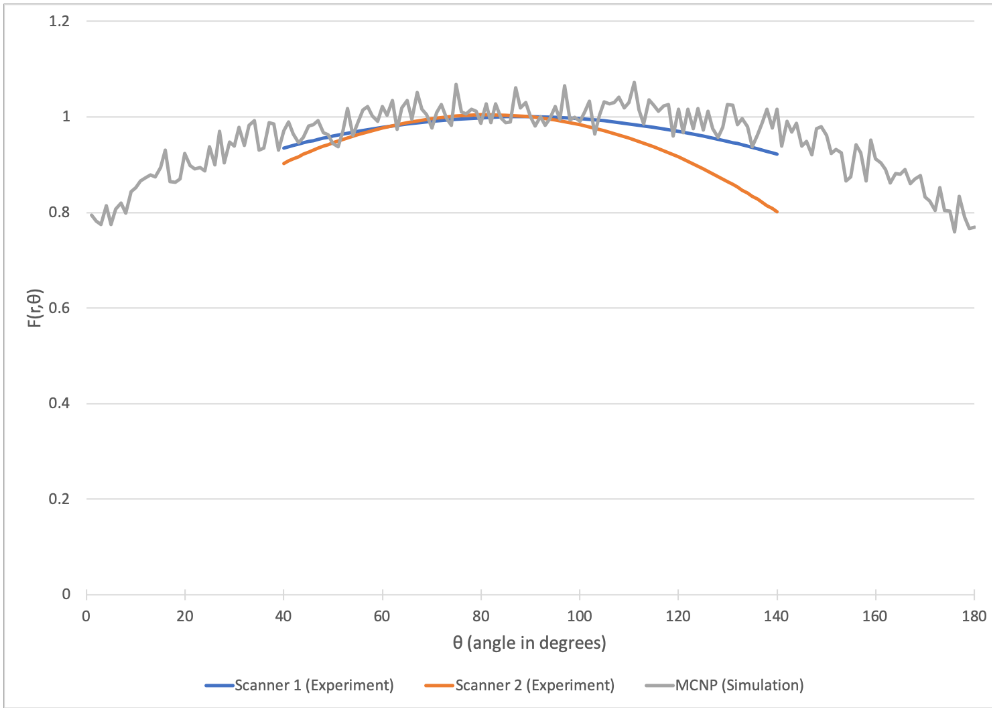

Figure 3.11: Anisotropy function at r=10 cm obtained from experiment and from simulation. The MCNP values are plotted against the values from Scanner 1 and Scanner 2.

3.D Air-kerma Strength and Dose-rate Constant

Since the F6-type tally outputs dose in MeV/g and the air-kerma strength calls for dose in cGy, a conversion factor of 1 cGy $= 6.242 * 10^7$ MeV/g was used. The output dose value for calculating the air-kerma strength was $7.3377 * 10^{-6}$ MeV/g with a percent error of 2.13%.

No conversion of dose units was done in calculating the dose-rate constant, which lacks any dose unit when simplified. The output dose value for calculating the dose-rate constant was $8.1407 * 10^{-4}$ MeV/g with a percent error of 0.42%.

$$S_K = 7.0532 * 10^{-12} \text{ cGy}\cdot\text{cm}^2/\text{h} \qquad \Lambda = 1.1094 \text{ cm}^{-2}$$

3.E Discussion

The radial dose function as depicted is not as smooth as what would be expected of a true function. The trend for $g(r)$ for this seed is roughly a parabolic curve with a maximum around $r = 5$. Perhaps a smoother curve could be obtained if the dose at every radius was measured individually rather than all at once, especially given that in the experiment the films were exposed one at a time to the seed. Of course using smaller radii increments in MCNP would yield more data points for the construction of a radial dose function, even though the experiment could only accommodate measurements at ten fixed radii.

For the experimental anisotropy measurements, we discovered a source of systematic error. Specifically, unintended asymmetry in exposing the films to the seed arose from complications with the afterloader and catheter. Despite our use of a computer to program the afterloader to push the seed a specified distance through the catheter, the seed would occasionally end up relatively far from the center of the film holder structure; furthermore, we observed that the catheter itself would sometimes bend or kink. The net effect was that the seed would not be in the ideal position and orientation for dose measurements at times. Thus, in comparing experimental anisotropy to MCNP anisotropy, percent differences are consistently larger at the edges of the film, i.e. the regions from 40° to 50° and 130° to 140°, than anywhere else. At greater radii, one edge may show much higher percent differences than the opposite edge, an occurrence best explained by the inaccurate, off-center placement of the seed.

Further error arose from how we fit certain films into the film holder. For the films exposed at 1 cm, 5 cm, and 6 cm, we had to cut notches in the films to allow the catheter to pass through without bending or kinking as much. These cuts caused the edges of the film to split, so our dosimetry produced inconsistently irradiated films. Even higher error occurred in measuring dose at the edges of the 1 cm, 5 cm, and 6 cm films, and the percent differences of MCNP anisotropy values from experimental anisotropy values for those films are significantly larger than those percent differences for the other films.

Noise in the MCNP measurements also sporadically triggers sharp spikes or dips in percent differences, but with the percent error of all dose measurements in these MCNP simulations being $<3\%$, the noise is trivial enough to be considered expected randomness. While the exceptionally high percent differences show that the experimental design can be much improved, the percent differences on the portions of the films that had not split show that the anisotropy functions found in the experiment are sufficiently similar to MCNP results to be considered reliable.

Not much can be said of the air-kerma strength without a reference, but the calculated dose-rate constant has a 0.41% difference from the manufacturer's value of 1.114 cm^{-2} (5). Considering that the percent error of the dose measurement for calculating the dose-rate constant is not only trivial but also approximately the same as the percent difference, the two values for the dose-rate constant are practically equivalent.

4 Conclusions

Comparison of the anisotropy results produced from the Monte Carlo simulations with those produced from the experiment show that it is possible to accurately characterize the parameters of the M-19 seed source using Gafchromic film dosimetry. The results from MCNP runs could be potentially improved by more exactly replicating the source geometry, altering the mesh cell dimensions, or properly defining the physical layout and material composition of Gafchromic film and the film holder.

Future work with this MCNP model would entail changing the source parameters to find the TG-43 parameters for another seed, particularly one with ytterbium or another low-energy source. Furthermore, the extra unused data, such as that from the FMESH tally, can serve as an alternative or complementary basis for results expected from future Gafchromic film dosimetry.

These results, in conjunction with other experiments to measure the air-kerma strength, dose-rate constant, and the radial dose function, can be used for FDA approval of this particular brachytherapy source. This source can therefore be used clinically.

References

[1] Alain; Pötter, Richard; Mazeron, Jean-Jacques; Meertens, Harm; Limbergen, Erik Van, eds. (2002). The GEC ESTRO handbook of brachytherapy. *Leuven, Belgium: European Society for Therapeutic Radiology and Oncology.*.

[2] Baes, F. (n.d.). Hps.org. Retrieved April 20, 2018, from http://hps.org/publicinformation/ate/faqs/gammaandexposure.html.

[3] Cameron, J. (1991). "Radiation Dosimetry." *Environmental Health Perspectives*, 91, pp.45-48.

[4] "ENSDF Decay Data in the MIRD (Medical Internal Radiation Dose) Format for 192Ir." (2000, May 18). Retrieved April 24, 2018, from https://www.orau.org/ptp/ptp library/library/doe/bnl/nuclidedata/MIRIr192.htm.

[5] "ESTRO Organisation Structure." ESTRO, ESTRO, https://www.estro.org/about/governance-organisation/committees-activities/tg43-ir-192-hdr.

[6] Fong, K. B., & Beinstein, N. E. (2018). Measuring the Anisotropy Function of Iridium-192 using Gafchromic Film Dosimetry. Retrieved from https://digitalcommons.wpi.edu/mqp-all/216.

[7] Flynn A, et al. (2005). "Isotopes and delivery systems for brachytherapy." In Hoskin P, Coyle C. *Radiotherapy in practice: brachytherapy.* New York: Oxford University Press.

[8] "Gafchromic$^{\text{TM}}$ Dosimetry Media, Type EBT-3." International Specialty Products Ashland Inc, 2014.

[9] Kairn, T., Aland, T., & Kenny, J. (2010). "Local heterogeneities in early batches of EBT2 film: a suggested solution." *Physics in medicine and biology*, 55 (15), L37.

[10] Mazeron, J. J., Ardiet, J. M., Haie-Méder, C., Kovács, G. R., Levendag, P.; Peiffert, D., Polo, A.; Rovirosa, A., Strnad, V. (2009). "GEC-ESTRO recommendations

for brachytherapy for head and neck squamous cell carcinomas." *Radiotherapy and Oncology*, 91 (2), pp.150–156.

[11] Moule, R. N.; Hoskin, P. J. (2009). "Non-surgical treatment of localised prostate cancer." *Surgical Oncology*, 18 (3), pp.255–267.

[12] Nag S. "A Brief Essay on the Introduction of Brachytherapy." Retrieved April 25, 2018, from https://www.americanbrachytherapy.org/aboutbrachytherapy/history.cfm.

[13] Nath, R., Anderson, L. L., Luxton, G., Weaver, K. A., Williamson, J. F., & Meigooni, A. S. (1995). "Dosimetry of Interstitial Brachytherapy Sources: Recommendation of the AAPM Radiation Therapy Committee Task Group 43." Medical Physics, 22 (2), pp.209-234.

[14] Radioisotope Brief: Iridium-192 (Ir-192). (2014, October 16). Retrieved April 24, 2018, from https://emergency.cdc.gov/radiation/isotopes/iridium.asp.

[15] Recommended Data, http://www.nucleide.org/DDEP_WG/DDEPdata.htm.

[16] Rivard, M., Coursey, B., DeWerd, L., Hanson, W., Saiful Huq, M., Ibbott, G., Mitch, M., Nath, R., & Williamson, J. (2004). "Update of AAPM Task Group No. 43 Report: A revised AAPM protocol for brachytherapy dose calculations." Medical Physics, 31 (3), pp.633-674.

[17] T. Goorley, et al., "Initial MCNP6 Release Overview", Nuclear Technology, 180, pp 298-315 (Dec 2012).

[18] "The Visual Editor for MCNP." The Visual Editor for MCNPX, Schwarz Software & Consulting, Richland, Washington, USA, Apr. 2018, http://www.mcnpvised.com/visualeditor/visualeditor.html.

[19] Thomadsen, B. R., et al. (2005). "Brachytherapy Physics." Medical Physics Publishing.

[20] Turner, J.E. (2007). "Atoms, radiation, and radiation protection." John Wiley & Sons.

Appendix A MCNP Codes

A.A Early Version of Main Code

```
c Cell Cards
10 1 -1.0 -2 1      imp:p,e=1     $inside "film" (film is actually about
half the cylindrical surface)
20 1 -1.0 -3 (-1:2) imp:p,e=1     $inside tank but outside film
30 0      3         imp:p,e=0     $outside tank/end of world

c Surface Cards
1 cx 0.95                       $inner layer of "film" (infinite cylinder
used to prevent superposition on surface 2)
2 rcc -10 0 0  20 0 0  1.05     $outer layer of "film" (assuming film is
about 1 mm thick, 20 cm wide, and 1 cm radially from the source)
3 rpp -50 50 -50 50 -50 50      $cubic tank of water (100 cm side length)

c Data Cards
mode p
F06:p     10
c
c Source Data
sdef par=p axs=1 0 0 ext=d1 rad=0 erg=0.38     $line source/seed (about
0.35 cm long) along x-axis centered at origin
si1 -0.175 0.175                               $xmin and xmax of seed
sp1 -21  0
c  sp1                                         $energy spectrum of Ir-192
c  sp2
c Materials Data
m1 1000 -0.11190 8000 -0.88810      $water is the only medium of interest
nps 10000
```

A.B Final Version of Main Code

```
c Column 81 just after asterisk                                                 *
c Cell Cards
110 1 -0.997 -112 111 11 -12     imp:p,e=1     $inside "film" placed 1 cm away f
rom source center
120 1 -0.997 -122 121 11 -12     imp:p,e=1     $2 cm
130 1 -0.997 -132 131 11 -12     imp:p,e=1     $3 cm
140 1 -0.997 -142 141 11 -12     imp:p,e=1     $4 cm
150 1 -0.997 -152 151 11 -12     imp:p,e=1     $5 cm
160 1 -0.997 -162 161 11 -12     imp:p,e=1     $6 cm
170 1 -0.997 -172 171 11 -12     imp:p,e=1     $7 cm
180 1 -0.997 -182 181 11 -12     imp:p,e=1     $8 cm
190 1 -0.997 -192 191 11 -12     imp:p,e=1     $9 cm
100 1 -0.997 -102 101 11 -12     imp:p,e=1     $10 cm
200 2 -7.80  -202 201            imp:p,e=1     $steel capsule of seed
210 0        -201 301            imp:p,e=1     $void between capsule and source
300 3 -22.4  -301                imp:p,e=1     $iridium source
400 1 -0.997 (-401 202)        &
             (-111:112:12:-11) &
             (-121:122:12:-11) &
             (-131:132:12:-11) &
             (-141:142:12:-11) &
             (-151:152:12:-11) &
             (-161:162:12:-11) &
             (-171:172:12:-11) &
             (-181:182:12:-11) &
             (-191:192:12:-11) &
             (-101:102:12:-11)   imp:p,e=1     $inside tank but outside seed and
             films
410 0         401                imp:p,e=0     $outside tank/end of world

c Surface Cards
c r=1 cm
111 cz 0.95           $inner surface of "film"
112 cz 1.05           $outer surface of "film" (assuming film is 1 mm thick)
c r=2 cm
121 cz 1.95           $inner surface
122 cz 2.05           $outer surface
c r=3 cm
131 cz 2.95
132 cz 3.05
c r=4 cm
141 cz 3.95
142 cz 4.05
```

```
c r=5 cm
151 cz 4.95
152 cz 5.05
c r=6 cm
161 cz 5.95
162 cz 6.05
c r=7 cm
171 cz 6.95
172 cz 7.05
c r=8 cm
181 cz 7.95
182 cz 8.05
c r=9 cm
191 cz 8.95
192 cz 9.05
c r=10 cm
101 cz 9.95
102 cz 10.05
c bases for the cylinders; film is 20 cm wide
11 pz -10
12 pz  10
c
201 rcc -0.176 0 0  0.352 0 0  0.0355   $inner surface of steel capsule
202 rcc -0.255 0 0  0.510 0 0  0.0585   $outer surface of steel capsule
301 rcc -0.175 0 0  0.350 0 0  0.0325   $cylindrical iridium pellet
401 rpp -50 50 -50 50 -50 50            $cubic tank of water (100 cm side length
)

c Data Cards
mode p
F16:p     110
F26:p     120
F36:p     130
F46:p     140
F56:p     150
F66:p     160
F76:p     170
F86:p     180
F96:p     190
F06:p     100     $this is the first tally listed in mctal
tmesh
cmesh13
cora13 0 0.95 1.05 1.95 2.05         $radii
corb13 -0.05 0.05                    $bases
corc13 0.5 179i 180.5 360            $angles
```

```
cmesh23
cora23 0 2.95 3.05 3.95 4.05
corb23 -0.05 0.05
corc23 0.5 179i 180.5 360
cmesh33
cora33 0 4.95 5.05 5.95 6.05
corb33 -0.05 0.05
corc33 0.5 179i 180.5 360
cmesh43
cora43 0 6.95 7.05 7.95 8.05
corb43 -0.05 0.05
corc43 0.5 179i 180.5 360
cmesh53
cora53 0 8.95 9.05 9.95 10.05
corb53 -0.05 0.05
corc53 0.5 179i 180.5 360
endmdd
*FMESH4:p   Geom = cyl   Origin = 0.0000 0.0000 -0.0500
            IMESH = 0.5 10.5             IINTS = 1 10
            JMESH = 0.1                  JINTS = 1
            KMESH = 0.001389 0.501389 1  KINTS = 1 180 1
            AXS= 0 0 1  VEC= 1 0 0  OUT = col
c
c Source Data
sdef par=2 axs=1 0 0 ext=d1 rad=d2 erg=d3      $cylindrical seed (0.35 cm long a
nd 0.065 cm in diameter) along x-axis centered at origin (by default)
si1 -0.175 0.175                               $xmin and xmax of pellet
sp1 -21  0
si2 0 0.0325                                   $rmin and rmax of pellet
sp2 -21  1
#       si3          sp3                       $energy spectrum of Ir-192
        L            D
       0.061486     0.012000
       0.063000     0.020500
       0.065122     0.026300
       0.066831     0.044600
       0.071079     0.002410
       0.071414     0.004660
       0.073363     0.001630
       0.075368     0.005330
       0.075749     0.010250
       0.077831     0.003650
       0.110400     0.000122
       0.136343     0.002000
       0.176980     0.000043
```

```
       0.201311     0.004730
       0.205794     0.033400
       0.280270     0.000090
       0.283267     0.002660
       0.295957     0.287200
       0.308455     0.296800
       0.316506     0.827100
       0.329170     0.000174
       0.374485     0.007260
       0.416469     0.006690
       0.420520     0.000690
       0.468069     0.478100
       0.484575     0.031870
       0.485300     0.000023
       0.489060     0.004380
       0.588581     0.045170
       0.593490     0.000421
       0.599410     0.000039
       0.604411     0.082000
       0.612462     0.053400
       0.703870     0.000053
       0.765800     0.000013
       0.884537     0.002910
       1.061480     0.000530
       1.089900     0.000012
       1.378200     0.000012
c
c Materials Data
m1      1000.04p  0.66667   8000.04p  0.33333                         $water
m2      6000.04p -0.00080   7000.04p -0.00100  14000.04p -0.00750 &
       15000.04p -0.00045  16000.04p -0.00030  24000.04p -0.17000 &
       25000.04p -0.02000  26000.04p -0.65495  28000.04p -0.12000 &
       42000.04p -0.02500                                             $Type 316
       Stainless Steel
m3     77000.04p -1.000                                               $iridium
c
prdmp 0 0 1
nps 100000000
```

A.C Supplementary Code for obtaining Air-kerma strength

```
c Cell Cards
110 1 -0.001184 -101                imp:p,e=1     $air point
120 1 -0.001184 -102                imp:p,e=1
200 2 -7.80     -202 201            imp:p,e=1     $steel capsule of seed
210 0           -201 301            imp:p,e=1     $void between capsule and sour
ce
300 3 -22.4     -301                imp:p,e=1     $iridium source
400 0           -401 101 102 202    imp:p,e=1     $vacuum around air point and s
eed
410 0            401                imp:p,e=0     $end of world

c Surface Cards
101 sy 10 0.05                          $sphere 10 cm from origin with 0.1 cm di
ameter
102 sy -1 0.05
201 rcc -0.176 0 0  0.352 0 0  0.0355   $inner surface of steel capsule
202 rcc -0.255 0 0  0.510 0 0  0.0585   $outer surface of steel capsule
301 rcc -0.175 0 0  0.350 0 0  0.0325   $cylindrical iridium pellet
401 so 100                              $edge of world

c Data Cards
mode p
F16:p     110
F26:p     120
c
c Source Data
sdef par=2 axs=1 0 0 ext=d1 rad=d2 erg=d3      $cylindrical seed (0.35 cm long a
nd 0.065 cm in diameter) along x-axis centered at origin (by default)
si1 -0.175 0.175                               $xmin and xmax of pellet
sp1 -21  0
si2 0 0.0325                                   $rmin and rmax of pellet
sp2 -21  1
#       si3          sp3                       $energy spectrum of Ir-192
        L            D
       0.061486     0.012000
       0.063000     0.020500
       0.065122     0.026300
       0.066831     0.044600
       0.071079     0.002410
       0.071414     0.004660
       0.073363     0.001630
       0.075368     0.005330
       0.075749     0.010250
```

```
       0.077831     0.003650
       0.110400     0.000122
       0.136343     0.002000
       0.176980     0.000043
       0.201311     0.004730
       0.205794     0.033400
       0.280270     0.000090
       0.283267     0.002660
       0.295957     0.287200
       0.308455     0.296800
       0.316506     0.827100
       0.329170     0.000174
       0.374485     0.007260
       0.416469     0.006690
       0.420520     0.000690
       0.468069     0.478100
       0.484575     0.031870
       0.485300     0.000023
       0.489060     0.004380
       0.588581     0.045170
       0.593490     0.000421
       0.599410     0.000039
       0.604411     0.082000
       0.612462     0.053400
       0.703870     0.000053
       0.765800     0.000013
       0.884537     0.002910
       1.061480     0.000530
       1.089900     0.000012
       1.378200     0.000012
c
cut:p  1j  0.001
cut:e  1j  0.020
c
c Materials Data
m1 6000 -0.00012 7000 -0.75527 8000 -0.23178 18000 -0.01283 GAS=1      $air
m2      6000.04p -0.00080   7000.04p -0.00100  14000.04p -0.00750 &
       15000.04p -0.00045  16000.04p -0.00030  24000.04p -0.17000 &
       25000.04p -0.02000  26000.04p -0.65495  28000.04p -0.12000 &
       42000.04p -0.02500                                          $Type 316
       Stainless Steel
m3     77000.04p -1.000                                            $iridium
c
prdmp 0 0 1
ctme 100
```

A.D Supplementary Code for obtaining Dose-rate constant

```
c Cell Cards
110 1 -0.997    -101                imp:p,e=1     $measurement point
200 2 -7.80     -202 201            imp:p,e=1     $steel capsule of seed
210 0           -201 301            imp:p,e=1     $void between capsule and sour
ce
300 3 -22.4     -301                imp:p,e=1     $iridium source
400 1 -0.997    -401 101 202        imp:p,e=1     $water around point and seed
410 0            401                imp:p,e=0     $end of world

c Surface Cards
101 sy 1 0.05                           $sphere 1 cm from origin with 0.1 cm dia
meter
201 rcc -0.176 0 0  0.352 0 0  0.0355   $inner surface of steel capsule
202 rcc -0.255 0 0  0.510 0 0  0.0585   $outer surface of steel capsule
301 rcc -0.175 0 0  0.350 0 0  0.0325   $cylindrical iridium pellet
401 so 100                              $edge of world

c Data Cards
mode p
F6:p     110
c
c Source Data
sdef par=2 axs=1 0 0 ext=d1 rad=d2 erg=d3      $cylindrical seed (0.35 cm long a
nd 0.065 cm in diameter) along x-axis centered at origin (by default)
si1 -0.175 0.175                               $xmin and xmax of pellet
sp1 -21  0
si2 0 0.0325                                   $rmin and rmax of pellet
sp2 -21  1
#       si3          sp3                       $energy spectrum of Ir-192
        L            D
       0.061486     0.012000
       0.063000     0.020500
       0.065122     0.026300
       0.066831     0.044600
       0.071079     0.002410
       0.071414     0.004660
       0.073363     0.001630
       0.075368     0.005330
       0.075749     0.010250
       0.077831     0.003650
       0.110400     0.000122
       0.136343     0.002000
       0.176980     0.000043
```

```
       0.201311     0.004730
       0.205794     0.033400
       0.280270     0.000090
       0.283267     0.002660
       0.295957     0.287200
       0.308455     0.296800
       0.316506     0.827100
       0.329170     0.000174
       0.374485     0.007260
       0.416469     0.006690
       0.420520     0.000690
       0.468069     0.478100
       0.484575     0.031870
       0.485300     0.000023
       0.489060     0.004380
       0.588581     0.045170
       0.593490     0.000421
       0.599410     0.000039
       0.604411     0.082000
       0.612462     0.053400
       0.703870     0.000053
       0.765800     0.000013
       0.884537     0.002910
       1.061480     0.000530
       1.089900     0.000012
       1.378200     0.000012
c
cut:p  1j  0.001
cut:e  1j  0.020
c
c Materials Data
m1      1000.04p  0.66667   8000.04p  0.33333                          $water
m2      6000.04p -0.00080   7000.04p -0.00100  14000.04p -0.00750 &
       15000.04p -0.00045  16000.04p -0.00030  24000.04p -0.17000 &
       25000.04p -0.02000  26000.04p -0.65495  28000.04p -0.12000 &
       42000.04p -0.02500                                          $Type 316
       Stainless Steel
m3     77000.04p -1.000                                            $iridium
c
prdmp 0 0 1
ctme 100
```

Appendix B Geometry Function

Table B.1: Geometry function times distance squared at radii 1 cm to 5 cm.

radius / angle	1	2	3	4	5
40	1.01365	1.00343	1.00153	1.00086	1.00055
41	1.01292	1.00325	1.00145	1.00082	1.00052
42	1.01220	1.00308	1.00137	1.00077	1.00049
43	1.01147	1.00290	1.00129	1.00073	1.00047
44	1.01074	1.00272	1.00121	1.00068	1.00044
45	1.01002	1.00254	1.00113	1.00064	1.00041
46	1.00929	1.00236	1.00105	1.00059	1.00038
47	1.00857	1.00218	1.00097	1.00055	1.00035
48	1.00785	1.00200	1.00089	1.00050	1.00032
49	1.00714	1.00183	1.00082	1.00046	1.00029
50	1.00643	1.00165	1.00074	1.00042	1.00027
55	1.00300	1.00079	1.00036	1.00020	1.00013
60	0.99982	0.99999	1.00000	1.00000	1.00000
65	0.99697	0.99926	0.99967	0.99982	0.99988
70	0.99454	0.99864	0.99940	0.99966	0.99978
75	0.99258	0.99813	0.99917	0.99953	0.99970
80	0.99114	0.99776	0.99900	0.99944	0.99964
85	0.99027	0.99754	0.99890	0.99938	0.99960
90	0.98998	0.99746	0.99887	0.99936	0.99959
95	0.99027	0.99754	0.99890	0.99938	0.99960
100	0.99114	0.99776	0.99900	0.99944	0.99964
105	0.99258	0.99813	0.99917	0.99953	0.99970
110	0.99454	0.99864	0.99940	0.99966	0.99978
115	0.99697	0.99926	0.99967	0.99982	0.99988
120	0.99982	0.99999	1.00000	1.00000	1.00000
125	1.00300	1.00079	1.00036	1.00020	1.00013
130	1.00643	1.00165	1.00074	1.00042	1.00027
131	1.00714	1.00183	1.00082	1.00046	1.00029
132	1.00785	1.00200	1.00089	1.00050	1.00032
133	1.00857	1.00218	1.00097	1.00055	1.00035
134	1.00929	1.00236	1.00105	1.00059	1.00038
135	1.01002	1.00254	1.00113	1.00064	1.00041
136	1.01074	1.00272	1.00121	1.00068	1.00044
137	1.01147	1.00290	1.00129	1.00073	1.00047
138	1.01220	1.00308	1.00137	1.00077	1.00049
139	1.01292	1.00325	1.00145	1.00082	1.00052
140	1.01365	1.00343	1.00153	1.00086	1.00055

Table B.2: Geometry function times distance squared at radii 6 cm to 10 cm.

radius / **angle**	**6**	**7**	**8**	**9**	**10**
40	1.00038	1.00028	1.00021	1.00017	1.00014
41	1.00036	1.00027	1.00020	1.00016	1.00013
42	1.00034	1.00025	1.00019	1.00015	1.00012
43	1.00032	1.00024	1.00018	1.00014	1.00012
44	1.00030	1.00022	1.00017	1.00013	1.00011
45	1.00028	1.00021	1.00016	1.00013	1.00010
46	1.00026	1.00019	1.00015	1.00012	1.00009
47	1.00024	1.00018	1.00014	1.00011	1.00009
48	1.00022	1.00016	1.00013	1.00010	1.00008
49	1.00020	1.00015	1.00012	1.00009	1.00007
50	1.00018	1.00014	1.00010	1.00008	1.00007
55	1.00009	1.00007	1.00005	1.00004	1.00003
60	1.00000	1.00000	1.00000	1.00000	1.00000
65	0.99992	0.99994	0.99995	0.99996	0.99997
70	0.99985	0.99989	0.99992	0.99993	0.99995
75	0.99979	0.99985	0.99988	0.99991	0.99993
80	0.99975	0.99982	0.99986	0.99989	0.99991
85	0.99973	0.99980	0.99985	0.99988	0.99990
90	0.99972	0.99979	0.99984	0.99987	0.99990
95	0.99973	0.99980	0.99985	0.99988	0.99990
100	0.99975	0.99982	0.99986	0.99989	0.99991
105	0.99979	0.99985	0.99988	0.99991	0.99993
110	0.99985	0.99989	0.99992	0.99993	0.99995
115	0.99992	0.99994	0.99995	0.99996	0.99997
120	1.00000	1.00000	1.00000	1.00000	1.00000
125	1.00009	1.00007	1.00005	1.00004	1.00003
130	1.00018	1.00014	1.00010	1.00008	1.00007
131	1.00020	1.00015	1.00012	1.00009	1.00007
132	1.00022	1.00016	1.00013	1.00010	1.00008
133	1.00024	1.00018	1.00014	1.00011	1.00009
134	1.00026	1.00019	1.00015	1.00012	1.00009
135	1.00028	1.00021	1.00016	1.00013	1.00010
136	1.00030	1.00022	1.00017	1.00013	1.00011
137	1.00032	1.00024	1.00018	1.00014	1.00012
138	1.00034	1.00025	1.00019	1.00015	1.00012
139	1.00036	1.00027	1.00020	1.00016	1.00013
140	1.00038	1.00028	1.00021	1.00017	1.00014

Appendix C Anisotropy Values

Table C.1: MCNP anisotropy at radii 1 cm to 10 cm.

radius / angle	1	2	3	4	5	6	7	8	9	10
40	0.9448	0.9833	0.9778	0.9691	0.9601	0.9521	0.9610	0.9578	0.9202	0.9717
41	0.9492	0.9625	0.9838	1.0037	0.9790	0.9681	1.0020	1.0025	0.9548	0.9888
42	0.9537	0.9526	0.9661	0.9389	0.9294	0.9454	0.9697	0.9698	0.9256	0.9644
43	0.9455	0.9499	0.9581	0.9768	0.9431	0.9405	0.9537	0.9694	0.9389	0.9455
44	0.9639	0.9764	0.9672	0.9628	0.9702	0.9566	0.9552	0.9645	0.9319	0.9564
45	0.9550	0.9824	0.9892	0.9853	0.9657	0.9624	0.9722	1.0071	0.9487	0.9805
46	0.9565	0.9363	0.9749	0.9806	0.9543	0.9620	0.9659	0.9966	0.9452	0.9839
47	0.9687	0.9795	0.9452	0.9412	0.9363	0.9505	0.9627	0.9542	0.9261	0.9922
48	0.9678	0.9764	0.9882	1.0117	0.9689	0.9447	0.9556	0.9843	0.9423	0.9672
49	0.9630	0.9777	0.9795	0.9793	0.9578	0.9615	0.9799	0.9947	0.9409	0.9626
50	0.9843	0.9600	0.9844	0.9895	0.9699	0.9530	0.9624	0.9855	0.9418	0.9452
55	0.9877	1.0109	1.0055	1.0187	1.0141	0.9994	1.0118	1.0420	1.0311	0.9864
60	0.9799	1.0173	1.0106	1.0087	0.9818	0.9595	0.9917	0.9944	0.9741	1.0223
65	1.0047	1.0091	0.9997	1.0001	0.9838	1.0005	1.0047	0.9906	1.0069	1.0348
70	1.0044	1.0250	1.0223	1.0110	1.0059	0.9978	1.0072	0.9917	0.9809	0.9773
75	0.9912	1.0126	1.0019	1.0178	0.9948	0.9843	1.0008	1.0070	0.9970	1.0685
80	1.0052	1.0114	1.0084	1.0223	0.9752	0.9831	0.9737	1.0115	0.9601	0.9868
85	0.9932	1.0211	1.0122	1.0284	1.0179	1.0148	1.0038	1.0080	0.9365	0.9874
90	1.0000	1.0000	1.0000	1.0000	1.0000	1.0000	1.0000	1.0000	1.0000	1.0000
95	1.0055	0.9937	0.9982	1.0053	0.9919	0.9926	0.9991	1.0553	0.9844	1.0218
100	1.0077	1.0097	1.0222	0.9969	0.9940	1.0030	1.0069	1.0254	0.9461	0.9912
105	0.9986	1.0050	1.0249	1.0495	1.0208	1.0211	1.0075	1.0304	0.9509	1.0309
110	1.0167	1.0279	1.0057	1.0346	1.0075	0.9932	1.0243	1.0391	0.9612	1.0297
115	0.9902	1.0225	1.0050	0.9893	0.9995	0.9723	0.9704	1.0310	0.9688	1.0238
120	0.9888	0.9788	0.9694	0.9731	0.9827	0.9521	0.9635	0.9852	0.9568	1.0159
125	0.9842	0.9927	0.9915	1.0149	0.9859	0.9760	0.9702	0.9878	0.9525	0.9727
130	0.9829	0.9869	0.9991	0.9760	0.9949	0.9945	0.9742	0.9932	0.9516	1.0254
131	0.9795	1.0007	0.9788	0.9756	0.9578	0.9656	1.0027	1.0394	0.9856	1.0248
132	0.9591	0.9737	1.0228	1.0295	0.9906	0.9722	1.0140	1.0106	0.9549	0.9837
133	0.9658	0.9836	0.9839	0.9969	0.9724	0.9692	0.9723	1.0061	0.9658	0.9970
134	0.9677	0.9642	0.9704	0.9716	0.9795	0.9626	0.9995	0.9720	0.9342	0.9799
135	0.9702	0.9743	0.9716	0.9794	0.9448	0.9426	0.9586	0.9425	0.9219	0.9376
136	0.9690	0.9973	0.9687	0.9796	0.9635	0.9490	0.9697	0.9786	0.9444	0.9625
137	0.9648	0.9785	0.9844	0.9622	0.9595	0.9457	0.9565	0.9865	0.9488	0.9881
138	0.9519	0.9601	0.9734	0.9639	0.9468	0.9198	0.9610	0.9822	0.9310	1.0162
139	0.9436	0.9527	0.9659	0.9768	0.9381	0.9473	0.9558	0.9783	0.9095	0.9772
140	0.9540	0.9545	0.9420	0.9545	0.9655	0.9439	0.9798	0.9958	1.0031	1.0164

Table C.2: Percent difference of MCNP anisotropy results from Scanner 1 results.

radius / **angle**	**1**	**2**	**3**	**4**	**5**	**6**	**7**	**8**	**9**	**10**
40	-35.07%	12.55%	-11.27%	10.17%	35.78%	3.90%	21.17%	16.51%	-15.61%	3.90%
41	-34.29%	9.60%	-10.57%	13.55%	37.46%	5.60%	25.40%	21.13%	-12.30%	5.43%
42	-33.50%	7.92%	-12.03%	5.71%	29.57%	3.09%	20.48%	16.43%	-14.84%	2.53%
43	-33.60%	7.08%	-12.60%	9.48%	30.54%	2.50%	17.65%	15.64%	-13.48%	0.26%
44	-31.81%	9.53%	-11.61%	7.42%	33.32%	4.20%	17.00%	14.35%	-13.99%	1.14%
45	-31.95%	9.69%	-9.44%	9.45%	31.76%	4.77%	18.27%	18.66%	-12.30%	3.42%
46	-31.36%	4.06%	-10.59%	8.46%	29.27%	4.66%	16.71%	16.73%	-12.48%	3.51%
47	-29.97%	8.37%	-13.15%	3.66%	25.93%	3.33%	15.56%	11.12%	-14.11%	4.13%
48	-29.53%	7.55%	-9.04%	10.97%	29.39%	2.62%	13.97%	13.96%	-12.46%	1.26%
49	-29.37%	7.23%	-9.68%	6.98%	26.99%	4.36%	16.13%	14.53%	-12.46%	0.54%
50	-27.28%	4.85%	-9.06%	7.68%	27.69%	3.34%	13.35%	12.84%	-12.22%	-1.50%
55	-24.31%	8.28%	-6.26%	8.87%	28.86%	7.79%	15.73%	16.30%	-3.10%	1.73%
60	-22.09%	7.15%	-4.89%	6.11%	20.45%	2.79%	10.47%	8.48%	-7.69%	4.50%
65	-17.08%	4.76%	-5.01%	3.78%	16.56%	6.31%	9.28%	5.89%	-3.76%	5.00%
70	-13.92%	5.13%	-1.91%	3.71%	15.12%	5.00%	7.25%	4.14%	-5.43%	-1.41%
75	-11.75%	2.86%	-2.91%	3.44%	10.02%	2.47%	4.56%	4.12%	-3.01%	7.32%
80	-7.00%	1.97%	-1.27%	3.13%	4.26%	1.10%	0.05%	3.21%	-5.75%	-1.17%
85	-4.48%	2.42%	0.14%	3.19%	5.23%	2.97%	1.65%	1.71%	-7.22%	-1.26%
90	0.00%	0.00%	0.00%	0.00%	0.00%	0.00%	0.00%	0.00%	0.00%	0.00%
95	4.57%	-0.71%	0.92%	0.38%	-4.02%	-2.29%	-1.14%	4.79%	-0.61%	2.32%
100	8.99%	1.03%	4.51%	-0.41%	-6.89%	-2.90%	-1.23%	1.31%	-3.55%	-0.46%
105	12.31%	0.93%	6.00%	5.08%	-7.41%	-2.89%	-1.85%	1.49%	-2.09%	3.98%
110	18.86%	3.83%	5.25%	4.04%	-11.47%	-7.31%	-0.70%	2.24%	-0.03%	4.45%
115	20.28%	4.12%	6.44%	0.11%	-14.90%	-11.01%	-6.23%	1.53%	1.79%	4.60%
120	24.70%	0.70%	3.93%	-0.71%	-18.89%	-14.64%	-7.03%	-2.72%	1.59%	4.71%
125	28.73%	3.43%	7.65%	4.62%	-21.09%	-14.33%	-6.35%	-2.00%	2.22%	1.31%
130	33.18%	4.36%	9.87%	1.86%	-22.76%	-14.60%	-5.77%	-0.82%	3.24%	8.07%
131	33.63%	6.18%	7.91%	2.10%	-26.09%	-17.46%	-2.95%	3.96%	7.16%	8.29%
132	31.75%	3.66%	13.06%	8.04%	-24.01%	-17.27%	-1.79%	1.25%	4.06%	4.23%
133	33.57%	5.08%	9.04%	4.92%	-25.86%	-17.89%	-5.75%	0.97%	5.48%	5.92%
134	34.73%	3.38%	7.82%	2.56%	-25.76%	-18.82%	-3.04%	-2.27%	2.25%	4.40%
135	35.98%	4.85%	8.24%	3.71%	-28.82%	-20.87%	-6.92%	-5.06%	1.12%	0.18%
136	36.71%	7.72%	8.20%	4.06%	-27.84%	-20.71%	-5.75%	-1.22%	3.83%	3.14%
137	36.99%	6.09%	10.25%	2.54%	-28.57%	-21.34%	-6.94%	-0.22%	4.54%	6.20%
138	36.03%	4.52%	9.30%	3.07%	-29.94%	-23.85%	-6.39%	-0.44%	2.82%	9.55%
139	35.70%	4.14%	8.75%	4.80%	-30.99%	-21.95%	-6.79%	-0.62%	0.67%	5.69%
140	38.05%	4.77%	6.34%	2.78%	-29.39%	-22.59%	-4.33%	1.39%	11.28%	10.27%

Table C.3: Percent difference of MCNP anisotropy results from Scanner 2 results.

radius / angle	1	2	3	4	5	6	7	8	9	10
40	-36.10%	-2.76%	-9.16%	-0.01%	22.70%	-15.96%	11.49%	12.93%	-0.14%	7.62%
41	-35.32%	-4.84%	-8.54%	3.34%	24.37%	-14.32%	15.54%	17.51%	3.24%	8.93%
42	-34.52%	-5.84%	-10.12%	-3.53%	17.39%	-16.10%	11.16%	13.03%	-0.28%	5.69%
43	-34.59%	-6.13%	-10.79%	0.18%	18.43%	-16.32%	8.71%	12.36%	0.79%	3.10%
44	-32.81%	-3.53%	-9.86%	-1.45%	21.12%	-14.66%	8.26%	11.19%	-0.31%	3.79%
45	-32.93%	-2.95%	-7.73%	0.67%	19.88%	-13.91%	9.60%	15.47%	1.15%	5.90%
46	-32.32%	-7.52%	-8.98%	0.01%	17.78%	-13.72%	8.31%	13.67%	0.45%	5.77%
47	-30.93%	-3.27%	-11.67%	-4.17%	14.91%	-14.53%	7.40%	8.29%	-1.89%	6.20%
48	-30.47%	-3.59%	-7.57%	2.83%	18.26%	-14.83%	6.07%	11.14%	-0.48%	3.08%
49	-30.29%	-3.47%	-8.30%	-0.62%	16.25%	-13.09%	8.24%	11.77%	-0.93%	2.16%
50	-28.20%	-5.23%	-7.74%	0.27%	17.07%	-13.63%	5.81%	10.21%	-1.12%	-0.09%
55	-25.14%	-0.22%	-5.25%	2.53%	19.17%	-8.25%	8.84%	13.97%	6.84%	2.42%
60	-22.82%	0.44%	-4.18%	0.99%	12.44%	-10.77%	4.70%	6.65%	-0.18%	4.61%
65	-17.72%	-0.29%	-4.55%	-0.26%	9.91%	-5.79%	4.40%	4.42%	2.25%	4.69%
70	-14.45%	1.40%	-1.65%	0.59%	9.72%	-4.87%	3.32%	3.00%	-1.08%	-1.94%
75	-12.15%	0.36%	-2.80%	1.17%	6.05%	-5.00%	1.61%	3.27%	0.04%	6.64%
80	-7.27%	0.48%	-1.26%	1.67%	1.69%	-3.97%	-1.88%	2.65%	-3.95%	-1.74%
85	-4.61%	1.75%	0.12%	2.48%	3.90%	0.31%	0.63%	1.44%	-6.42%	-1.62%
90	0.00%	0.00%	0.00%	0.00%	0.00%	0.00%	0.00%	0.00%	0.00%	0.00%
95	4.71%	-0.22%	1.01%	1.03%	-2.76%	0.40%	-0.09%	5.07%	-1.29%	2.85%
100	9.26%	1.87%	4.76%	0.83%	-4.39%	2.59%	0.94%	1.85%	-4.69%	0.75%
105	12.71%	1.94%	6.49%	7.00%	-3.61%	5.59%	1.51%	2.30%	-3.57%	6.13%
110	19.38%	4.89%	6.04%	6.50%	-6.54%	3.79%	3.99%	3.33%	-1.68%	7.72%
115	20.89%	5.01%	7.63%	2.98%	-8.86%	2.68%	-0.47%	2.89%	0.16%	9.21%
120	25.39%	1.24%	5.56%	2.59%	-11.86%	1.56%	0.12%	-1.14%	0.19%	10.89%
125	29.48%	3.47%	9.91%	8.56%	-12.98%	5.13%	2.41%	-0.13%	1.26%	9.08%
130	33.94%	3.70%	12.86%	6.11%	-13.54%	8.15%	4.77%	1.37%	2.93%	18.62%
131	34.39%	5.34%	11.00%	6.44%	-17.02%	5.20%	8.28%	6.32%	7.00%	19.36%
132	32.48%	2.67%	16.45%	12.72%	-14.43%	6.12%	9.96%	3.60%	4.07%	15.37%
133	34.30%	3.90%	12.46%	9.55%	-16.26%	5.99%	5.91%	3.38%	5.68%	17.76%
134	35.46%	2.03%	11.37%	7.16%	-15.90%	5.46%	9.35%	0.12%	2.63%	16.59%
135	36.70%	3.28%	11.97%	8.43%	-19.12%	3.46%	5.37%	-2.67%	1.70%	12.40%
136	37.41%	5.90%	12.10%	8.87%	-17.76%	4.34%	7.09%	1.32%	4.63%	16.28%
137	37.68%	4.10%	14.39%	7.36%	-18.34%	4.17%	6.15%	2.42%	5.57%	20.32%
138	36.69%	2.33%	13.60%	7.98%	-19.66%	1.49%	7.19%	2.25%	4.05%	24.74%
139	36.34%	1.73%	13.21%	9.87%	-20.63%	4.70%	7.15%	2.13%	2.11%	20.97%
140	38.67%	2.11%	10.88%	7.82%	-18.54%	4.51%	10.43%	4.26%	13.15%	26.89%

Appendix D Raw TMESH Data

Table D.1: Dose (MeV/cm^3/source particle) and percent error at radii 1 cm to 5 cm.

radius	**1**		**2**		**3**		**4**		**5**	
angle	Dose	Error	Dose	Error	Dose	Error	Dose	Error	Dose	Error
40	7.81E-04	0.89%	2.00E-04	1.27%	8.83E-05	1.54%	4.91E-05	1.75%	3.16E-05	1.92%
41	7.84E-04	0.88%	1.96E-04	1.28%	8.88E-05	1.54%	5.08E-05	1.73%	3.23E-05	1.91%
42	7.87E-04	0.88%	1.94E-04	1.29%	8.72E-05	1.54%	4.75E-05	1.76%	3.06E-05	1.95%
43	7.80E-04	0.88%	1.93E-04	1.28%	8.65E-05	1.55%	4.94E-05	1.74%	3.11E-05	1.92%
44	7.94E-04	0.87%	1.99E-04	1.28%	8.73E-05	1.55%	4.87E-05	1.75%	3.20E-05	1.91%
45	7.87E-04	0.88%	2.00E-04	1.27%	8.93E-05	1.52%	4.99E-05	1.73%	3.18E-05	1.92%
46	7.87E-04	0.88%	1.90E-04	1.29%	8.80E-05	1.53%	4.96E-05	1.74%	3.14E-05	1.92%
47	7.97E-04	0.87%	1.99E-04	1.27%	8.53E-05	1.55%	4.76E-05	1.76%	3.08E-05	1.92%
48	7.95E-04	0.87%	1.98E-04	1.26%	8.92E-05	1.53%	5.12E-05	1.72%	3.19E-05	1.92%
49	7.91E-04	0.87%	1.99E-04	1.26%	8.84E-05	1.53%	4.96E-05	1.73%	3.15E-05	1.92%
50	8.08E-04	0.86%	1.95E-04	1.28%	8.88E-05	1.52%	5.01E-05	1.73%	3.19E-05	1.90%
55	8.08E-04	0.85%	2.05E-04	1.25%	9.07E-05	1.51%	5.15E-05	1.72%	3.34E-05	1.87%
60	7.99E-04	0.86%	2.06E-04	1.24%	9.11E-05	1.51%	5.10E-05	1.72%	3.23E-05	1.91%
65	8.17E-04	0.85%	2.05E-04	1.24%	9.01E-05	1.51%	5.06E-05	1.73%	3.24E-05	1.90%
70	8.14E-04	0.84%	2.08E-04	1.24%	9.21E-05	1.50%	5.11E-05	1.71%	3.31E-05	1.89%
75	8.02E-04	0.85%	2.05E-04	1.23%	9.03E-05	1.51%	5.15E-05	1.71%	3.27E-05	1.88%
80	8.12E-04	0.84%	2.05E-04	1.24%	9.08E-05	1.50%	5.17E-05	1.70%	3.21E-05	1.89%
85	8.02E-04	0.85%	2.07E-04	1.24%	9.12E-05	1.51%	5.20E-05	1.71%	3.35E-05	1.86%
90	8.07E-04	0.85%	2.02E-04	1.25%	9.01E-05	1.51%	5.06E-05	1.72%	3.29E-05	1.88%
95	8.12E-04	0.84%	2.01E-04	1.25%	8.99E-05	1.52%	5.08E-05	1.72%	3.27E-05	1.90%
100	8.14E-04	0.84%	2.04E-04	1.24%	9.21E-05	1.49%	5.04E-05	1.72%	3.27E-05	1.89%
105	8.08E-04	0.84%	2.03E-04	1.24%	9.24E-05	1.50%	5.31E-05	1.68%	3.36E-05	1.86%
110	8.24E-04	0.84%	2.08E-04	1.23%	9.06E-05	1.51%	5.23E-05	1.70%	3.32E-05	1.88%
115	8.05E-04	0.85%	2.07E-04	1.24%	9.06E-05	1.52%	5.00E-05	1.73%	3.29E-05	1.88%
120	8.06E-04	0.85%	1.99E-04	1.26%	8.74E-05	1.53%	4.92E-05	1.74%	3.24E-05	1.89%
125	8.05E-04	0.86%	2.02E-04	1.25%	8.94E-05	1.52%	5.13E-05	1.72%	3.25E-05	1.88%
130	8.07E-04	0.87%	2.01E-04	1.26%	9.02E-05	1.52%	4.94E-05	1.75%	3.28E-05	1.89%
131	8.04E-04	0.87%	2.03E-04	1.26%	8.83E-05	1.54%	4.94E-05	1.75%	3.15E-05	1.92%
132	7.88E-04	0.87%	1.98E-04	1.27%	9.23E-05	1.51%	5.21E-05	1.72%	3.26E-05	1.92%
133	7.94E-04	0.87%	2.00E-04	1.26%	8.88E-05	1.53%	5.05E-05	1.74%	3.20E-05	1.93%
134	7.96E-04	0.87%	1.96E-04	1.27%	8.76E-05	1.54%	4.92E-05	1.75%	3.23E-05	1.90%
135	7.99E-04	0.87%	1.98E-04	1.27%	8.77E-05	1.54%	4.96E-05	1.74%	3.11E-05	1.93%
136	7.99E-04	0.87%	2.03E-04	1.26%	8.75E-05	1.55%	4.96E-05	1.75%	3.17E-05	1.91%
137	7.96E-04	0.88%	1.99E-04	1.28%	8.89E-05	1.53%	4.87E-05	1.76%	3.16E-05	1.91%
138	7.86E-04	0.88%	1.95E-04	1.28%	8.79E-05	1.54%	4.88E-05	1.75%	3.12E-05	1.94%
139	7.79E-04	0.89%	1.94E-04	1.28%	8.72E-05	1.55%	4.95E-05	1.75%	3.09E-05	1.93%
140	7.88E-04	0.88%	1.94E-04	1.28%	8.51E-05	1.55%	4.83E-05	1.76%	3.18E-05	1.92%

Table D.2: Dose (MeV/cm^3/source particle) and percent error at radii 6 cm to 10 cm.

radius	**6**		**7**		**8**		**9**		**10**	
angle	Dose	Error	Dose	Error	Dose	Error	Dose	Error	Dose	Error
40	2.17E-05	2.08%	1.57E-05	2.24%	1.17E-05	2.38%	9.15E-06	2.51%	7.40E-06	2.62%
41	2.20E-05	2.07%	1.64E-05	2.19%	1.23E-05	2.35%	9.49E-06	2.47%	7.53E-06	2.60%
42	2.15E-05	2.09%	1.59E-05	2.22%	1.19E-05	2.34%	9.20E-06	2.48%	7.35E-06	2.59%
43	2.14E-05	2.07%	1.56E-05	2.21%	1.18E-05	2.33%	9.33E-06	2.48%	7.20E-06	2.63%
44	2.18E-05	2.06%	1.56E-05	2.21%	1.18E-05	2.35%	9.26E-06	2.48%	7.29E-06	2.63%
45	2.19E-05	2.08%	1.59E-05	2.23%	1.23E-05	2.33%	9.43E-06	2.48%	7.47E-06	2.64%
46	2.19E-05	2.05%	1.58E-05	2.22%	1.22E-05	2.32%	9.40E-06	2.46%	7.50E-06	2.59%
47	2.16E-05	2.08%	1.58E-05	2.21%	1.17E-05	2.37%	9.21E-06	2.47%	7.56E-06	2.56%
48	2.15E-05	2.10%	1.56E-05	2.24%	1.20E-05	2.37%	9.37E-06	2.48%	7.37E-06	2.62%
49	2.19E-05	2.06%	1.60E-05	2.21%	1.22E-05	2.32%	9.35E-06	2.47%	7.33E-06	2.65%
50	2.17E-05	2.07%	1.58E-05	2.21%	1.20E-05	2.33%	9.36E-06	2.45%	7.20E-06	2.63%
55	2.28E-05	2.05%	1.66E-05	2.20%	1.27E-05	2.33%	1.03E-05	2.40%	7.52E-06	2.62%
60	2.18E-05	2.07%	1.62E-05	2.20%	1.22E-05	2.34%	9.68E-06	2.43%	7.79E-06	2.57%
65	2.28E-05	2.05%	1.64E-05	2.18%	1.21E-05	2.34%	1.00E-05	2.40%	7.88E-06	2.53%
70	2.27E-05	2.05%	1.65E-05	2.18%	1.21E-05	2.34%	9.75E-06	2.45%	7.45E-06	2.60%
75	2.24E-05	2.03%	1.64E-05	2.18%	1.23E-05	2.31%	9.91E-06	2.41%	8.14E-06	2.50%
80	2.24E-05	2.03%	1.59E-05	2.18%	1.24E-05	2.31%	9.54E-06	2.44%	7.52E-06	2.60%
85	2.31E-05	2.02%	1.64E-05	2.18%	1.23E-05	2.33%	9.31E-06	2.48%	7.52E-06	2.59%
90	2.28E-05	2.03%	1.64E-05	2.19%	1.22E-05	2.34%	9.94E-06	2.42%	7.62E-06	2.61%
95	2.26E-05	2.05%	1.64E-05	2.22%	1.29E-05	2.30%	9.78E-06	2.45%	7.78E-06	2.56%
100	2.28E-05	2.04%	1.65E-05	2.18%	1.25E-05	2.33%	9.40E-06	2.47%	7.55E-06	2.57%
105	2.32E-05	2.00%	1.65E-05	2.17%	1.26E-05	2.29%	9.45E-06	2.45%	7.85E-06	2.54%
110	2.26E-05	2.05%	1.68E-05	2.18%	1.27E-05	2.32%	9.55E-06	2.47%	7.84E-06	2.57%
115	2.21E-05	2.06%	1.59E-05	2.22%	1.26E-05	2.29%	9.63E-06	2.45%	7.80E-06	2.53%
120	2.17E-05	2.09%	1.58E-05	2.24%	1.20E-05	2.36%	9.51E-06	2.45%	7.74E-06	2.58%
125	2.22E-05	2.04%	1.59E-05	2.20%	1.21E-05	2.33%	9.47E-06	2.45%	7.41E-06	2.57%
130	2.26E-05	2.03%	1.60E-05	2.22%	1.21E-05	2.35%	9.46E-06	2.46%	7.81E-06	2.56%
131	2.20E-05	2.08%	1.64E-05	2.19%	1.27E-05	2.31%	9.80E-06	2.44%	7.81E-06	2.55%
132	2.21E-05	2.07%	1.66E-05	2.20%	1.24E-05	2.34%	9.49E-06	2.49%	7.50E-06	2.64%
133	2.21E-05	2.07%	1.59E-05	2.21%	1.23E-05	2.32%	9.60E-06	2.47%	7.60E-06	2.60%
134	2.19E-05	2.07%	1.64E-05	2.17%	1.19E-05	2.36%	9.29E-06	2.48%	7.47E-06	2.58%
135	2.15E-05	2.08%	1.57E-05	2.20%	1.15E-05	2.36%	9.17E-06	2.47%	7.14E-06	2.65%
136	2.16E-05	2.09%	1.59E-05	2.23%	1.20E-05	2.37%	9.39E-06	2.47%	7.33E-06	2.62%
137	2.15E-05	2.08%	1.57E-05	2.22%	1.21E-05	2.36%	9.43E-06	2.48%	7.53E-06	2.57%
138	2.09E-05	2.12%	1.57E-05	2.22%	1.20E-05	2.36%	9.26E-06	2.53%	7.74E-06	2.57%
139	2.16E-05	2.08%	1.57E-05	2.22%	1.20E-05	2.33%	9.04E-06	2.50%	7.45E-06	2.61%
140	2.15E-05	2.10%	1.60E-05	2.22%	1.22E-05	2.36%	9.97E-06	2.46%	7.74E-06	2.60%

Appendix E Visual Editor Images

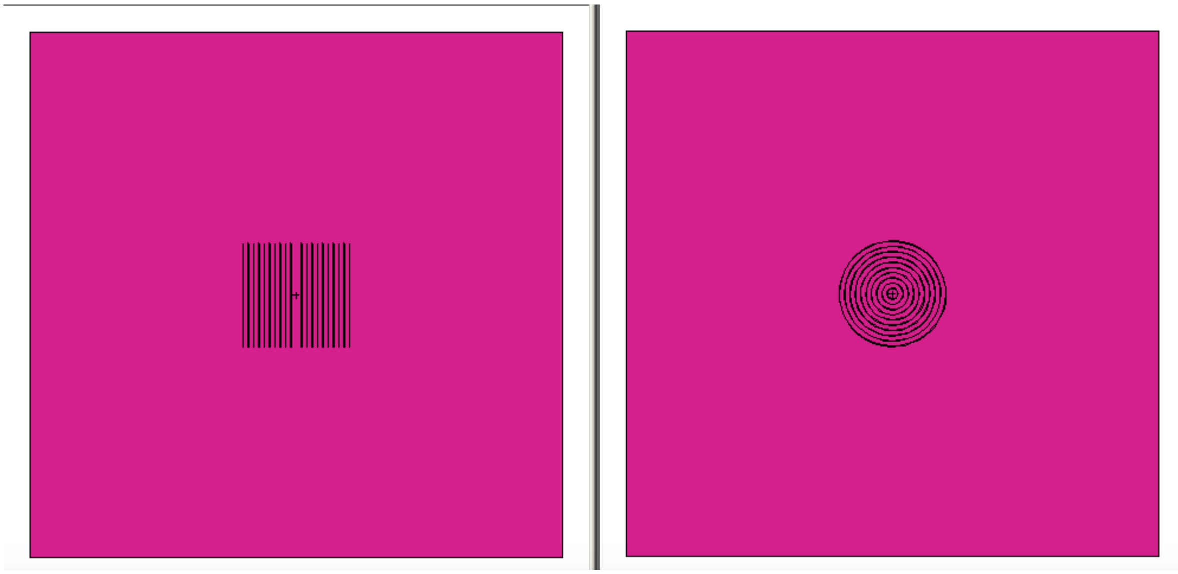

(a) View of the xz-plane at y=0. (b) View of the xy-plane at z=0.

Figure E.1: Images of the entire final MCNP model from a side view (a) and a top view (b). The magenta box represents the tank of water while the white space outside of it represents the vacuum of the particle graveyard. At the center are the ten cylindrical shells representing the films and the three volumes representing the seed (18).

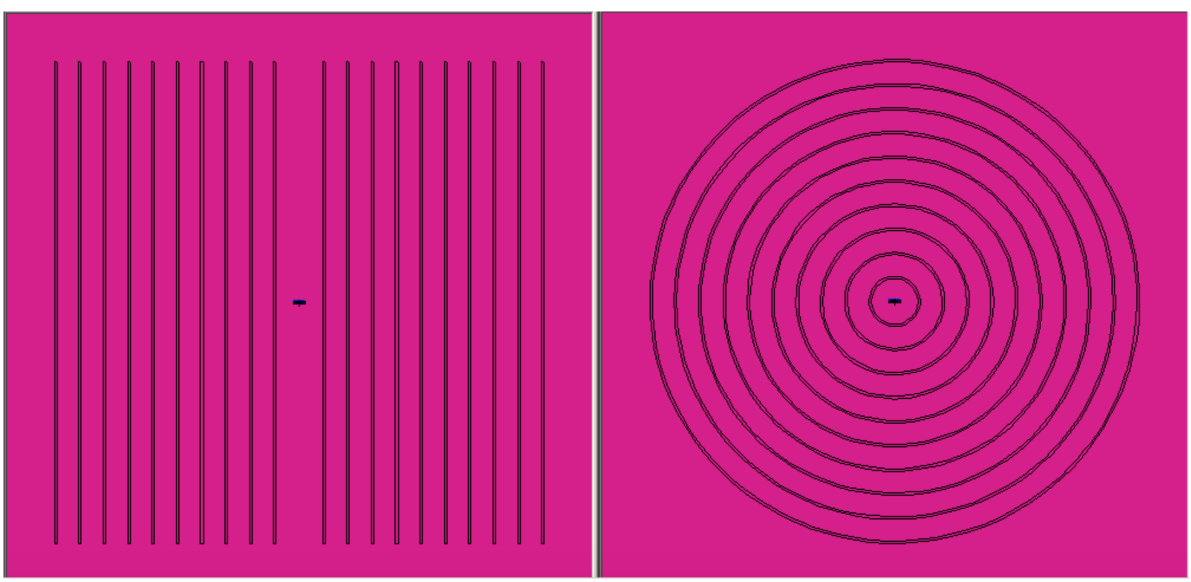

(a) View of the xz-plane at y=0. (b) View of the xy-plane at z=0.

Figure E.2: Images zoomed in on the ten films around the seed. (18).

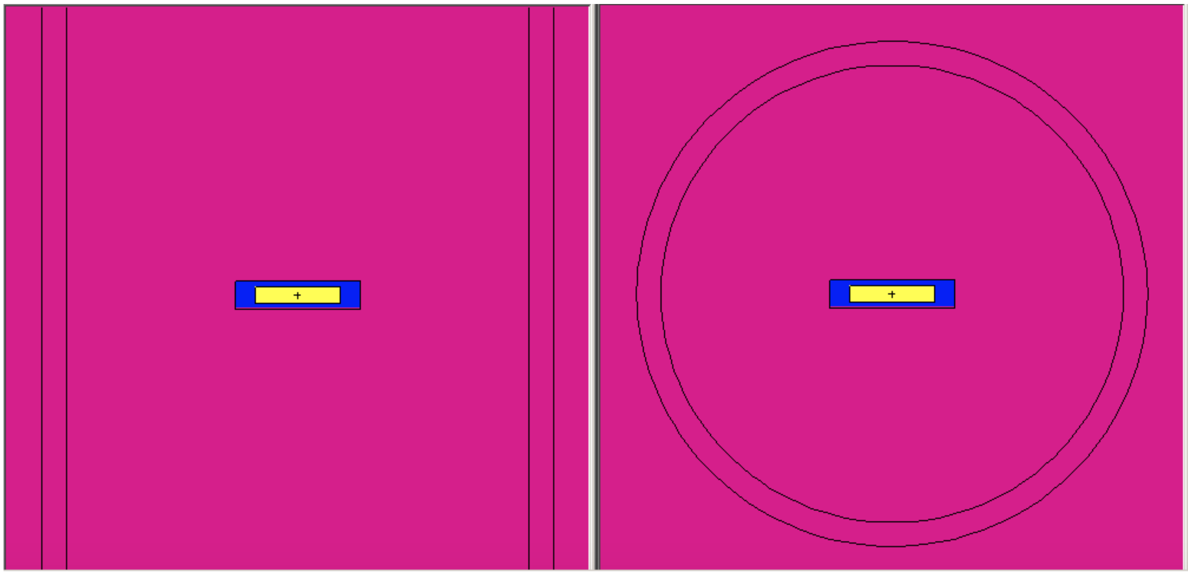

(a) View of the xz-plane at y=0. (b) View of the xy-plane at z=0.

Figure E.3: Images zoomed in on the 1 cm film and the seed. Note that the film has thickness and appears magenta like the tank since both consist of water. The seed consists of the yellow cylinder (iridium-192 pellet), the blue cylindrical shell (steel capsule) and the negligible white space between them (vacuum; not shown) (18).

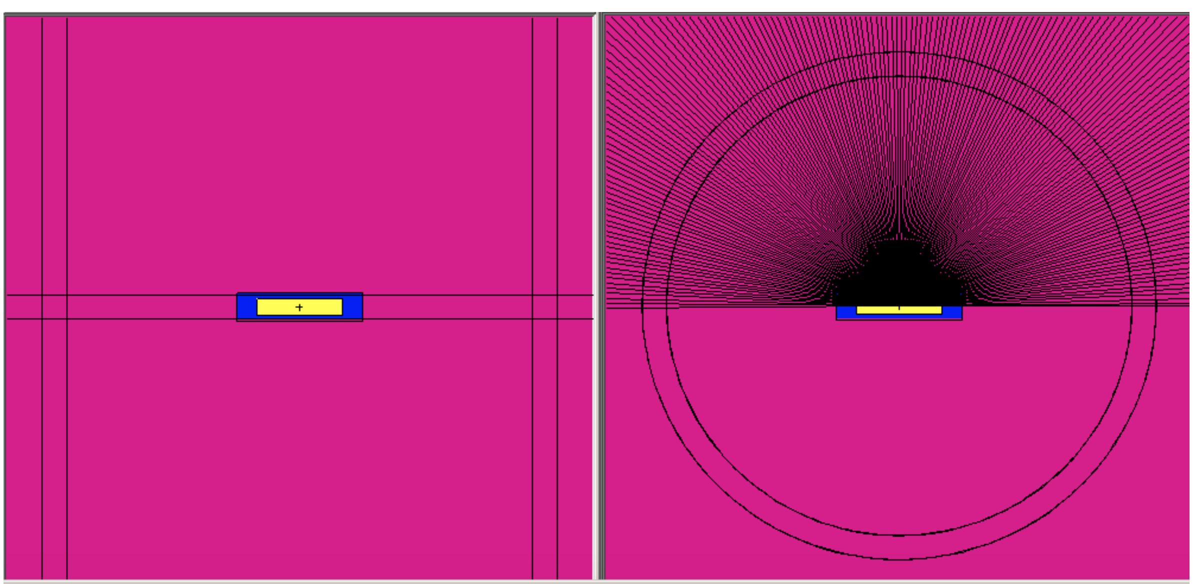

(a) View of the xz-plane at y=0. (b) View of the xy-plane at z=0.

Figure E.4: The same images from Figure E.3 overlaid with the TMESH cell boundaries. Note that the radial cell boundaries coincide with the edges of the film. The vertical cell boundaries can be seen in (a), and the angular cell boundaries can be seen in (b) (18).